FORSCHUNGSZENTRUM JÜLICH GmbH KFA

Institut für Plasmaphysik
Association EURATOM-KFA

2D model calculations of carbon density and radiation profiles within the minor cross-section of TEXTOR

H.A. Claaßen H. Gerhauser B. Mohamed

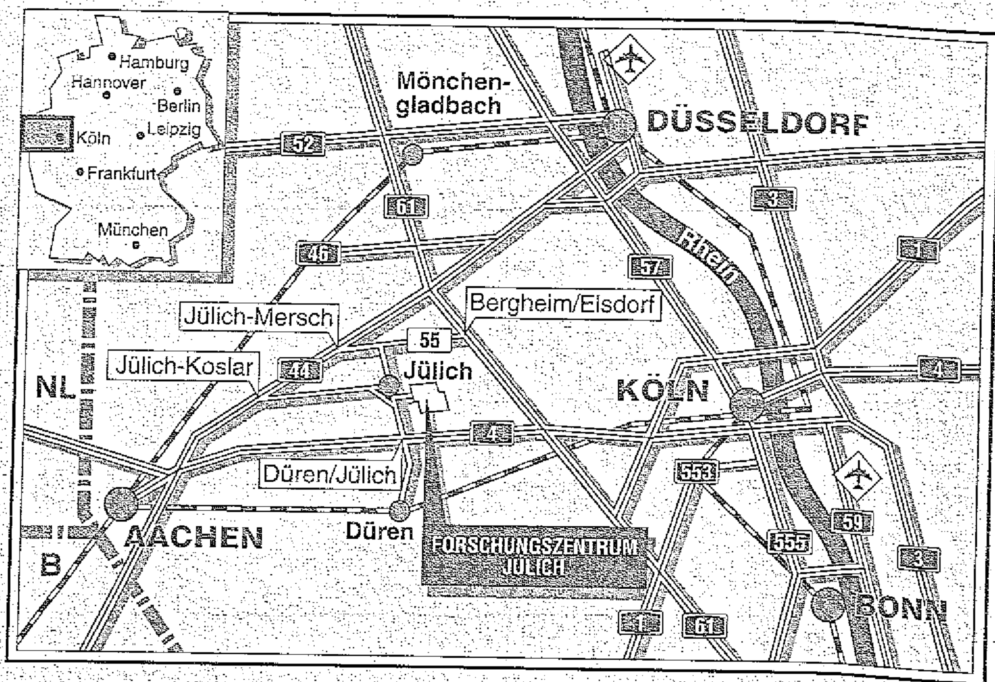

Berichte des Forschungszentrums Jülich ; 3058
ISSN 0944-2952
Institut für Plasmaphysik Jül-3058
Association EURATOM-KFA

Zu beziehen durch: Forschungszentrum Jülich GmbH · Zentralbibliothek
D-52425 Jülich · Bundesrepublik Deutschland
Telefon: 02461/61-6102 · Telefax: 02461/61-6103 · Telex: 833556-70 kfa d

2D model calculations of carbon density and radiation profiles within the minor cross-section of TEXTOR

H.A. Claaßen H. Gerhauser B. Mohamed *

*permanent address: Plasma Physics Dept. NRC, AEA, Cairo, Egypt

In recent years a number of experimental investigations have been performed concerning the space distribution of carbon ions in the TEXTOR plasma. These measurements were either local (radial distribution of C^{z+}-ions at the outboard midplane as measured by Li^0-beam activated cx-spectroscopy [1]) or integral (spectral measurements of C^{z+}-line emission integrated along off-centered lines within an angular range as seen from a spectrometer at an upper position of the TEXTOR-vessel [2]). In discharges with carbon as the main impurity species also bolometric measurements [3] give some indications of the space distribution of carbon within the minor plasma cross-section. The comparison of the corresponding experimental observations with theory requires 2D-model calculations including the Shafranov-shifted magnetic field configuration and the poloidal ALT-II limiter position of TEXTOR (as schematically depicted in fig.1). Results of such calculations are discussed in the present paper.

Basic equations and approximations:

The starting point are the particle balance equations (using standard notation together with Q_n as particle source function and omitting here the subindex z to denote the charge state under consideration):

$$div\left[V_{\|}n\frac{\vec{B}}{B}-\left(n\vec{\nabla}\Phi+\frac{\vec{F}}{ze}\right)\times\frac{\vec{B}}{B^2}-D_{\perp}\vec{\nabla}_{\perp}n\right]=Q_n-(\nu_I+\nu_R)n\equiv S_n$$

$$\vec{F}\equiv Mn\vec{V}\bullet\vec{\nabla}\vec{V}+\vec{\nabla}p$$

$$Q_n=\begin{cases} Q_0+(\nu_R n)_2 & : \quad z=1 \\ (\nu_I n)_{z-1}+(\nu_R n)_{z+1} & : \quad 2\le z\le 5 \\ (\nu_I n)_5 & : \quad z=6 \end{cases}$$

describing the charge state distribution of carbon considered as a single trace impurity element in a given deuterium plasma background under steady-state conditions. ν_I and ν_R denote respectively the frequencies for electron impact ionization and radiative plus dielectronic recombination. Q_0 is the source function due to ionization of the carbon atoms. In the limit $\vec{V}_{\perp}=0=rot\vec{B}$ we may replace $\vec{F}$ by

$$\vec{F}\rightarrow\vec{\nabla}\left(\frac{1}{2}MnV_{\|}^2+p\right)\equiv\vec{\nabla}\Psi$$

In the above formulation the cross-field particle flux is restricted to contributions from electric, diamagnetic and centrifugal (as most important part of the inertial) drift motion as well as anomalous transport in radial direction (the physical origin of the different drift contributions is more clearly seen in a drift-kinetic approach [4]). By elimination of the divergence- free part of the diamagnetic drift we isolate its toroidal effect

$$div\Big(-\frac{\vec{\nabla}\Psi}{ze} \times \frac{\vec{B}}{B^2}\Big) = \vec{\nabla}\Psi \bullet rot\Big(\frac{\vec{B}}{zeB^2}\Big)$$

to form an effective source function

$$Q_{eff} = Q_n - \vec{\nabla}\Psi \bullet rot\Big(\frac{\vec{B}}{zeB^2}\Big)$$

Similarly, the toroidal effect of the electric drift may be separated by using the decomposition

$$div(\vec{V}_{\perp}^{E} n) = \vec{V}_{\perp}^{E} \bullet \vec{\nabla} n + zen\vec{\nabla}\Phi \bullet rot\Big(\frac{\vec{B}}{zeB^2}\Big) \quad ; \quad \vec{V}_{\perp}^{E} = -\frac{\vec{\nabla}\Phi \times \vec{B}}{B^2}$$

Note that in the $rot\vec{B} = 0$ approximation

$$rot\Big(\frac{\vec{B}}{zeB^2}\Big) = -\frac{2(\vec{\nabla}_{\perp} \ln B \times \vec{B})}{zeB^2}$$

with equal contributions from space variations of both the direction and the magnitude of $\vec{B}$.

The connection with the deuterium plasma background is given by the electrostatic field $-\vec{\nabla}\Phi$ and the plasma parameters determining the transport coefficients ($\perp \vec{B}$ due to plasma turbulence and $\|\vec{B}$ due to Coulomb collisions between impurity ions and deuterons as well as electrons, which mainly contribute to the thermal forces) and the source (loss) functions. The $\|\vec{B}$ influence is described by the balance equations for the parallel momentum

$$Mn\vec{V} \bullet \vec{\nabla} V_{\|} = -\nabla_{\|} p + zenE_{\|} + R_{\|} + (S_{p\|} - MV_{\|}S_n) - div(\overleftrightarrow{\Pi} \bullet \frac{\vec{B}}{B}) +$$

$$+(Mn\vec{V}_{\perp}\vec{V}_{\perp} + \overleftrightarrow{\Pi}) : \vec{\nabla}\frac{\vec{B}}{B} + MnV_{\|}\vec{V}_{\perp} \bullet \vec{\nabla}_{\perp} \ln B$$

where the last line of the equation describes the curvature effects in the $rot\vec{B} = 0$ approximation. The elastic and inelastic momentum transfer is given by the expressions (here and in the following, quantities referring to deuterons or electrons are denoted by the subindices + and - respectively):

$$R_{\|} = \Big[M\alpha\nu_C(V_{\|+} - V_{\|}) + z^2\nabla_{\|}(2.21kT_+ + 0.71kT_-)\Big]n$$

$$S_{p\|} - MV_{\|}S_n = M(\nu_I n)_{z-1}(V_{\|z-1} - V_{\|})$$

where $\alpha\nu_C$ denotes the momentum transfer frequency due to Coulomb collisions between impurity and deuterium ions. Recombination processes are omitted here, since they are negligible compared to either ionization (for low charge states) or Coulomb scattering (for higher charge states). $\overleftrightarrow{\Pi}$ is the dissipative part of the pressure tensor including anomalous viscosity contributions.

In passing to the limit $\vec{V}_{\perp} \to 0$ and $\overleftrightarrow{\Pi} \to 0$ we adopt in the following a simplified 1D-approximation of the momentum balance equations by completely neglecting the viscosity and field curvature as well as cross-field inertial effects. It should, however, be noted that anomalous diffusion and viscosity effects may become important near the separatrix, where naturally the cross-field gradients of $V_{||}$ become large. In the 1D approximation (without the longitudinal viscosity effect) the parallel momentum equation yields a linear variation of $V_{||}$ along $\vec{B}$ with $\nabla_{||}V_{||} = 1/\tau_{||} = const.$, if the driving forces also vary linearly along $\vec{B}$. This presupposes that the particle source function, which is concentrated near the limiter head and determines the pressure gradient predominantly in the region inside the separatrix, has a Gaussian profile with respect to the coordinate $||\vec{B}$. Such conditions, which are roughly fulfilled by the SOLXY-code results for the deuterium plasma background and supported by an appropriately chosen Gaussian source function for $z = 1$ (see below), may be considered as a zero-order approximation of an iterative solution procedure. We then obtain (using the abbreviation $M(\nu_I V_{||} n)_{z-1} \equiv Q_{p||}$ and going to the limit $(\nu_I n)_{z-1} = (\nu_I n)_z$ for all z in the momentum loss term):

$$Mn(\nu_I + \frac{1}{\tau_{||}})V_{||} = -\nabla_{||}p + zenE_{||} + R_{||} + Q_{p||}$$

which due to the pressure gradient transforms the particle balance equations into a system of elliptic differential equations.

Neglecting collisional cross-field effects, the influence of the plasma background on the cross-field motion of the impurity ions is reduced to the influence of the $\perp \vec{B}$ components of the electric field determining the electric drift and indirectly (via the electric field fluctuations) $D_\perp$. The DC-components of the electric field are a superposition of a flux-surface averaged radial component, which in the plasma core guarantees a flux-surface averaged (global) ambipolarity in radial direction, and a vertical component, which arises from the vertical drift motion of the charge carriers. Compared to the flux-surface averaged radial component, the latter is of the order $(B^2\nu_{C-})/(B_\theta^2\Omega_-) \ll 1$ due to the high electrical conductivity of the plasma in $||\vec{B}$ direction and is neglected in the present calculations. It should, however, be noted that the $||\vec{B}$ velocity of the background ions driven by the vertical drift according to $B\nabla_{||}(n_+V_{||+}/B) + (\vec{\nabla}\Psi_+ + en_+\vec{\nabla}\Phi) \bullet rot(\vec{B}/eB^2) \simeq 0$ with $\Psi_+ \simeq p_+$ for $|V_{||+}| \ll v_{T+}$ has been indirectly accounted for (see below), since it has a non-negligible influence on the vertical asymmetry of the impurity ion population due to the $\|\vec{B}$ friction force. The latter has to be compensated by an induced Lorentz force to satisfy the momentum balance in toroidal direction, and thereby generates a radial particle flux, which, when averaged over a magnetic flux surface, is described by the well-known neoclassical formula for the Pfirsch-Schlüter regime and the standard magnetic field configuration with concentric flux surfaces as already used in 1D calculations [5] (the standard formula is reduced by 1/2 for the presently considered magnetic field configuration with excentric flux surfaces → see next chapter). While a generally valid algebraic expression for the flux-surface averaged radial component of the electric field cannot be derived (it was shown recently [6] that this component has to compensate for inertial and gyroviscous forces in the presence of differential poloidal rotation due to the electric drift of the background ions and thus follows from a differential equation), we simply use here (apart from $E_\theta = 0$) the relation $E_r = (1/n_p e)\partial p_+/\partial r$, which follows from the assumption of vanishing poloidal rotation of the background ions. Although simultaneously causing $V_{\|+} \simeq 0$, it leads to the correct formula for the $\|\vec{B}$ friction force $F_\| = M\alpha\nu_C(V_{\|+} - V_\|)n \sim (zn/n_+)\partial p_+/\partial r - \partial p/\partial r$, which should not contain contributions from the electric drift. In passing to the very plasma edge, the current flow is strongly disturbed by the limiter, while still preserving the global ambipolarity constraint under steady-state conditions without biasing, and non-negligible electric field components both in radial and poloidal direction appear. These are taken from the SOLXY-code results.

Magnetic field configuration:

To simulate the TEXTOR-relevant magnetic field configuration, we introduce an axisymmetric coordinate system with the metric coefficients $ds_r = h_r dr$, $ds_\theta = rh_\theta^* d\theta$, and $ds_\phi = R_0 h_\phi^* d\phi$ with $R = R_0 h_\phi^*$ for an orthogonal coordinate system describing the magnetic surfaces of Shafranov-shifted tori, the projections of which onto a radial -poloidal (minor) cross section are horizontally shifted (excentric) circles. For the metric coefficients we obtain the approximate formulae:

$$h_r = \frac{1}{1 + \frac{r}{R_0}\cos\theta} \quad ; \quad h_\theta^* = \frac{1 + \frac{a}{R_0}\cos\theta}{1 + \frac{r}{R_0}\cos\theta}$$

$$h_\phi^* = 1 + \frac{1}{2}\Big(\frac{a-r}{R_0}\Big)^2 h_r + \frac{r}{R_0}\cos\theta \; h_\theta^*$$

where $h_r h_\phi^* = 1$, if we neglect terms of the order $\leq (a/R_0)^2$. In this coordinate system we have $\vec{B} = (0, -\Theta, 1/h_\phi^*)B_0$ with $\Theta = \Theta(r)$, if we assume $B_\phi h_\phi^* = const$, and $\partial B_\theta/\partial\theta = 0$, which follow from $rot\vec{B} = 0$ and $div\vec{B} = 0$ in the limit $h_r h_\phi^* = 1$. For the assumed axisymmetry $\partial/\partial\phi = 0$ the particle balance equations read:

$$\frac{\partial(r\Gamma_r^*)}{r\partial r} + \frac{\partial\Gamma_\theta^*}{r\partial\theta} = Q_{eff}^* - (\nu_I^* + \nu_R^*)n$$

$$\Gamma_r^* = (V_r^{A*} + V_r^{E*})n \quad ; \quad \Gamma_\theta^* = (-\Theta V_\parallel^* + V_\theta^{E*})n$$

$$Q_{eff}^* = Q_n^* + \frac{2}{zeB}\Big(\frac{\partial h_\phi^*}{\partial r}\frac{\partial\Psi}{r\partial\theta} - \frac{\partial h_\phi^*}{r\partial\theta}\frac{\partial\Psi}{\partial r}\Big)$$

which appear as written in a cylindrical coordinate system with modified particle velocities and sources (losses)

$$V_r^{A*} \equiv -D_\perp^* \frac{\partial \ln n}{\partial r} \quad ; \quad D_\perp^* \equiv \frac{D_\perp h_\theta^* h_\phi^*}{h_r} \quad ; \quad V_r^{E*} \equiv -\frac{h_\phi^{*2}}{B_0}\frac{\partial\Phi}{r\partial\theta}$$

$$V_\parallel^* \equiv V_\parallel h_r h_\phi^{*2} \quad ; \quad V_\theta^{E*} \equiv \frac{h_\phi^{*2}}{B_0}\frac{\partial\Phi}{\partial r}$$

$$Q_n^* - (\nu_I^* + \nu_R^*)n \equiv [Q_n - (\nu_I + \nu_R)n]h_r h_\theta^* h_\phi^*$$

In the following we assume a Gaussian line source of monoenergetic carbon atoms ($v_{T0} = \sqrt{2\varepsilon_0/M}$ with $\varepsilon_0 = 4eV$ for carbon sputtering by deuterons) at the separatrix $r = a$ with a maximum at $\theta_L^* = \theta_L + \Delta\theta$ and an exponential decay length λ

$$Q_0 = \Big(\frac{|\Gamma_{r0}|\nu_I}{v_{T0}}\Big)_{z=0} \exp\Big(-\frac{a^2(\theta-\theta_L^*)^2}{\lambda^2} - |\int_a^r \frac{\nu_I(r')dr'}{v_{T0}}|\Big)_{z=0}$$

The poloidal asymmetry of the deuteron flux onto the limiter is, in a rough approximation, taken into account by the shift $\Delta\theta$ with respect to the middle of the limiter head at $\theta_L = -\pi/4$. The formula for Q_0 ignores the flux compression for decreasing radius and the slightly curved orbits when following the lines $\theta = const.$ in a magnetic field configuration with excentric flux surfaces. Since the ionization length of the sputtered carbon atoms is rather short, the error thereby introduced may be neglected.

The reduced 1D form of the parallel momentum equation then reads

$$M\nu_{eff}^* V_\| n = Q_{p\|}^* - h_r h_\theta^* h_\phi^* \nabla_\| p +$$

$$+\Big[M\alpha\nu_C^* V_{\|+} + h_r h_\theta^* h_\phi^* (zeE_\| + 2.21z^2\nabla_\| kT_+ + 0.71z^2\nabla_\| kT_-)\Big]n$$

where

$$Q_{p\|,z}^* = M(\nu_I^* V_\| n)_{z-1} \quad ; \quad (\nu_{eff}n)_z = (\alpha\nu_C + \frac{1}{\tau_\|})_z n_z + (\nu_I n)_{z-1}$$

$$\rightarrow \nu_{eff} \simeq \alpha\nu_C + \nu_I + \frac{1}{\tau_\|} \quad \text{for} \quad (\nu_I n)_{z-1} = (\nu_I n)_z$$

$$(\alpha\nu_C^*, \nu_{eff}^*) \equiv h_r h_\theta^* h_\phi^* (\alpha\nu_C, \nu_{eff})$$

Since we assume an axisymmetric plasma configuration, we have $\nabla_\| = -\Theta h_\phi^* \partial / h_\theta^* r \partial\theta$. Whereas the first line of the parallel momentum equation describes the dominant effects for the lower charge states in the region inside the separatrix, the second line accounts for friction, electric and thermal forces, which strongly contribute to the momentum balance of the higher charge states within the scrape-off layer. The convection time $\tau_\|$ changes accordingly when crossing the separatrix. Within the present approximations $\tau_\|$ can only be roughly estimated (see Appendix I). With the above expression for $V_\|$ we finally obtain:

$$\Gamma_\theta^* = V_\theta^{eff*} n - D_\theta^* \frac{\partial n}{r\partial\theta} - q_\theta^* \quad ; \quad V_\theta^{eff*} = V_\theta^{E*} - \Theta h_r h_\phi^{*2} V_\|^0$$

$$V_\|^0 \equiv \frac{\alpha\nu_C}{\nu_{eff}} V_{\|+} + \frac{zeE_\| + (2.21z^2 - 1)\nabla_\| kT_+ + 0.71z^2 \nabla_\| kT_-}{M\nu_{eff}}$$

$$D_\theta^* \equiv \frac{D_\theta h_r h_\phi^*}{h_\theta^*} \quad ; \quad D_\theta \equiv \frac{\Theta^2 h_\phi^{*2} kT_+}{M\nu_{eff}} \quad ; \quad q_\theta^* \equiv \frac{\Theta h_\phi^* Q_{p\|}^*}{M\nu_{eff} h_\theta^*}$$

The average radial particle flux:

Without consideration of sources/sinks and anomalous diffusion we derive here the formula for the magnetic flux surface averaged radial particle flux in the present magnetic field configuration (a more complete derivation including sources/sinks and anomalous diffusion is given in ref.[4] for the standard magnetic field configuration). The corresponding reduced form of the particle balance equation reads

$$\frac{\Theta}{r}\frac{\partial}{\partial\theta}(h_\phi^* n V_\|) \simeq -\frac{2h_\phi^* \sin\theta}{zeB_0R_0}\Big(\frac{\partial p}{\partial r} + zen\frac{\partial\Phi}{\partial r}\Big)$$

neglecting the poloidal gradients of pressure and electrostatic potential to first order drift approximation. On integration with respect to θ we obtain

$$nV_{\|} = -\frac{2r(\int h^*_\phi \sin\theta \, d\theta + C)}{h^*_\phi ze\Theta B_0 R_0}\Big(\frac{\partial p}{\partial r} + zen\frac{\partial \Phi}{\partial r}\Big)$$

with an analogous formula for $n_+ V_{\|+}$. The integration constant C is given by the condition $\oint nV_{\|}(h^*_\theta d\theta/2\pi) = 0$, when integrated over a magnetic flux surface. If we use $\int h^*_\phi \sin\theta \, d\theta = -\cos\theta - (r/4R_0)(2\cos^2\theta - 1)$ and neglect contributions of the order $\leq (a/R_0)^2$ we get $C = (a-2r)/(2R_0)$. Now, the toroidal component of the friction force (exerted by the deuterons on the carbon ions) must be compensated by the Lorentz force such that

$$nV_r = -\frac{F^R_\phi}{zeB_\theta} \simeq \frac{Mn\alpha\nu_C}{ze\Theta B_0}(V_{\|+} - V_{\|})$$

By inserting the formulae for $V_{\|+}$ and $V_{\|}$ we get the expression

$$nV_r \simeq -\frac{M\alpha\nu_C}{(ze\Theta B_0)^2}\frac{2r(\int h^*_\phi \sin\theta \, d\theta + C)}{R_0 h^*_\phi}\Big(\frac{zn}{n_+}\frac{\partial p_+}{\partial r} - \frac{\partial p}{\partial r}\Big)$$

from which the electric drift terms have disappeared. Averaging over a magnetic flux surface $r = const.$ yields (in the limit $h_r h^*_\phi \simeq 1$)

$$< nV_r > \equiv \frac{\oint d\theta \, d\phi \; r h^*_\theta R_0 h^*_\phi n V_r}{\oint d\theta \, d\phi \; r h^*_\theta R_o h^*_\phi} \simeq \oint \frac{d\theta}{2\pi}(1 + \frac{a}{R_0}\cos\theta) \, nV_r$$

Performing the θ-integrations and using the value $C = (a - 2r)/(2R_0)$, we obtain within errors of the order $\leq (a/R_0)^2$ the final result

$$< nV_r > = \frac{M\alpha\nu_C q^2}{(zeB_0)^2}\Big(\frac{zn}{n_+}\frac{\partial p_+}{\partial r} - \frac{\partial p}{\partial r}\Big) \quad \text{with} \quad q = \frac{r}{\Theta R_0}$$

where we have introduced the safety factor q. The difference to the standard formula with $2q^2$ instead of q^2 may be traced back to the difference in the poloidal field, which here is constant over the magnetic flux surface, namely $B_\theta = -\Theta B_0$, in contrast to the standard model, where $B_\theta = -\Theta B_0/h^*_\phi$.

Limiter geometry and boundary conditions:

In order to avoid the introduction of periodic boundary conditions in the poloidal direction and to be consistent with the SOLXY-code calculations of the plasma background parameters, we evaluate the balance equations in a Cartesian coordinate system $x = r\cos\theta^*$ and $y = r\sin\theta^*$ (shown in fig.2 in connection with the circular integration domain). In this coordinate system the intersection of the toroidal belt limiter (ALT-II) with the minor plasma cross section is symmetrically divided by the x-axis at $\theta^* = 0$, whereas the outboard midplane position $\theta = 0$ appears at $\theta^* = \pi/4$. The vertical direction $R = const$ coincides with the straight line $y = -x$, i.e. all metric coefficients have to be related to $\theta = \theta^* - \pi/4$. With this transformation we finally obtain (introducing the gyrofrequency $\Omega = zeB/M$ and the thermal velocity $v_T = \sqrt{2kT_+/M}$):

$$\frac{\partial\Gamma^*_x}{\partial x} + \frac{\partial\Gamma^*_y}{\partial y} = Q^*_{eff} - (\nu^*_I + \nu^*_R)n$$

$$\Gamma^*_x = \frac{1}{r}\,(x\Gamma^*_r - y\Gamma^*_\theta) \quad ; \quad \Gamma^*_y = \frac{1}{r}\,(y\Gamma^*_r + x\Gamma^*_\theta)$$

$$Q^*_{eff} = Q^*_n - \frac{h^*_\phi}{\Omega R\sqrt{2}}\Big(\frac{\partial}{\partial x} - \frac{\partial}{\partial y}\Big)\Big((V^2_\parallel + v^2_T)n\Big)$$

By inserting the expressions for Γ_r^* and Γ_θ^* we finally obtain Γ_x^* and Γ_y^* in the form (for $Q_{p\|}^* = 0$):

$$\Gamma_x^* = -a_p \frac{\partial n}{\partial x} - b_p \frac{\partial n}{\partial y} + c_p n \quad ; \quad \Gamma_y^* = -a_s \frac{\partial n}{\partial x} - b_s \frac{\partial n}{\partial y} + c_s n$$

$$a_p = \frac{x^2 D_\perp^* + y^2 D_\theta^*}{r^2} \quad ; \quad a_s = \frac{xy(D_\perp^* - D_\theta^*)}{r^2}$$

$$b_p = \frac{xy(D_\perp^* - D_\theta^*)}{r^2} \quad ; \quad b_s = \frac{x^2 D_\theta^* + y^2 D_\perp^*}{r^2}$$

$$c_p = \frac{x V_r^{E*} - y V_\theta^{eff*}}{r} \quad ; \quad c_s = \frac{x V_\theta^{eff*} + y V_r^{E*}}{r}$$

These equations have been numerically evaluated by the finite element computer code PDE2D, using SOLXY-code results for the deuterium plasma edge profiles with an appropriate continuation into the plasma core (describing measured radial plasma profiles on the condition that the plasma parameters do not vary within a magnetic surface). As boundary conditions we choose $n = 0$ at the torus wall and prescribe the outward flux components (out of the integration domain) $\pm\Gamma_\theta^*$ at the ion/electron side of the limiter and $\Gamma_r^* = 0$ at the limiter head. The values of Γ_θ^* at the lateral sides of the limiter are derived (using the moment method to solve the drift-kinetic equation, see Appendix II) on the condition of complete ion absorption (i.e. no impurity ion reemission) at the limiter surface making the ion velocity distribution function one-sided. They pose a relation between the density and its spatial derivative perpendicular to the limiter plane. In a rough approximation we obtain (keeping in mind that $E_r = -\partial\Phi/h_r\partial r, \Gamma_\theta^* = h_r h_\phi^* \Gamma_\theta \simeq \Gamma_\theta$ and $V_\theta^{eff*} = -\Theta h_r h_\phi^{*2} v_T g$):

electron-side:

$$g \equiv \frac{V_{\|}^0}{v_T} + \frac{E_r}{\Theta v_T B_0} \gtrless 0 \qquad \text{depending on magnitude and sign of } V_{\|}^0$$

$$\Gamma_\theta = -\frac{\Theta h_\phi^* \exp(-g^2) v_T n}{\sqrt{\pi}(1 - \mathrm{erf} g)} \leq 0$$

with the limiting values

$$g \to +\infty : \qquad \Gamma_\theta \to -\Theta h_\phi^* g v_T n < 0 \qquad \to \text{suprathermal flow}$$

$$g \to 0 : \qquad \Gamma_\theta \to -\frac{\Theta h_\phi^* v_T n}{\sqrt{\pi}} < 0 \qquad \to \text{subthermal flow } (\Theta h_\phi^* \ll 1)$$

$$g \to -\infty : \qquad \Gamma_\theta \to 0 \qquad \to \text{stagnation}$$

For $\Theta h_\phi^* g < 1$ we encounter subthermal flow towards the limiter or even convective flow reversal in the sense that $g < 0$ resp. $\Theta V_{\|}^0 B_0 < -E_r$ due to the thermoforces. Since Γ_θ is approximated by a superposition of a convective part $(V_\theta^E - \Theta h_\phi^* V_{\|}^0)n$ and a diffusive part $-D_\theta \partial n / h_\theta^* r \partial\theta$, we obtain (introducing the longitudinal diffusion coefficient $D_{\|} = kT_+/M\nu_{eff} = D_\theta/(\Theta h_\phi^*)^2$)

$$-D_{\|} \frac{\partial n}{\partial x_{\|}} = -\left[g - \frac{\exp(-g^2)}{\sqrt{\pi}(1 - \mathrm{erf} g)}\right] v_T n \geq 0$$

with the limiting values $\qquad g \to +\infty : \quad \dfrac{\partial n}{\partial x_{\|}} \to 0$

$$g \to 0: \quad \frac{\partial n}{\partial x_{\|}} \to -\frac{v_T n}{D_{\|}\sqrt{\pi}} < 0 \qquad ; \qquad g \to -\infty: \quad \frac{\partial n}{\partial x_{\|}} \to \frac{g v_T n}{D_{\|}} < 0$$

<u>ion-side</u>:

$$g \equiv \frac{V_{\|}^0}{v_T} + \frac{E_r}{\Theta v_T B_0} \lesseqgtr 0 \qquad \text{depending on magnitude and sign of } V_{\|}^0$$

$$\Gamma_\theta = \frac{\Theta h_\phi^* \exp(-g^2) v_T n}{\sqrt{\pi}(1 + \mathrm{erf} g)} \geq 0$$

with the limiting values

$$g \to -\infty: \qquad \Gamma_\theta \to -\Theta h_\phi^* g v_T n > 0 \qquad \to \text{suprathermal flow}$$

$$g \to 0: \qquad \Gamma_\theta \to \frac{\Theta h_\phi^* v_T n}{\sqrt{\pi}} > 0 \qquad \to \text{subthermal flow } (\Theta h_\phi^* \ll 1)$$

$$g \to +\infty: \qquad \Gamma_\theta \to 0 \qquad \to \text{stagnation}$$

$g > 0$ presupposes $\Theta V_{\|}^0 B_0 > -E_r$. The density gradient $\|\vec{B}$ is given by

$$-D_{\|}\frac{\partial n}{\partial x_{\|}} = -\left[g + \frac{\exp(-g^2)}{\sqrt{\pi}(1 + \mathrm{erf} g)}\right] v_T n \leq 0$$

with the limiting values $\qquad g \to -\infty: \quad \dfrac{\partial n}{\partial x_{\|}} \to 0$

$$g \to 0: \quad \frac{\partial n}{\partial x_{\|}} \to \frac{v_T n}{D_{\|}\sqrt{\pi}} > 0 \qquad ; \qquad g \to +\infty: \quad \frac{\partial n}{\partial x_{\|}} \to \frac{g v_T n}{D_{\|}} > 0$$

The functions $F^{\pm}(g) \equiv g \pm \exp(-g^2)/\sqrt{\pi}(1 \pm \mathrm{erf} g)$ determining the $\|\vec{B}$ density gradients in front of the lateral surfaces of the limiter (with $\pm$ corresponding to the ion/electron side) are shown in fig.3.

Results and discussion:

Fig.4 shows the density and line radiation distribution of the various carbon charge states $C^{z+}(2 \leq z \leq 6)$ over the minor cross section of the TEXTOR plasma. In order to save computation time, we have skipped the first charge state from the system of transport equations making use of the approximate ionization equilibrium $Q_0 = (\nu_I n)_0 \simeq (\nu_I n)_1$ at the plasma edge. The density and (ion/electron) temperature profiles of the deuterium plasma background used as input data for the calculations combine approximate fits of the 1D plasma profiles as measured for the plasma interior for a typical Ohmic discharge and low-Z (C-O) plasma contamination with the 2D plasma edge profiles from SOLXY-code calculations [7]. The anomalous diffusion coefficient is assumed to obey an ALCATOR-like scaling $D_{\perp} = 2 * 10^{18}/n_p$ (in MKSA- units) ignoring any poloidal dependence. The input data for the Gaussian line source of limiter released carbon are chosen in such a way as to fit the total C^0 particle outflux $\lambda\sqrt{\pi}\Gamma_{r0}2\pi R$ from the head of the toroidal belt limiter and the emission energy to the experimental values $\simeq 7.54 \times 10^{19}/sec$ and $4eV$ (yielding $\Gamma_{r0} \simeq 2.33 \times 10^{19}/(m^2 sec)$ in case of $\lambda = a\Delta\theta = 0.14m$ for the poloidal half-width of the limiter head). In order to get a better agreement with the measured C^{z+}-density profiles at the outboard midplane, we added to the limiter source an equal contribution from a uniform wall emission flux density $2.18 \times 10^{18}/(m^2 s)$ of carbon atoms. The emission energy of wall released carbon is reduced to $1eV$ to simulate to some extent source contributions from carbon containing molecular species.

The C^{z+} density and line radiation profiles show the characteristic features of radial shell structure and poloidal asymmetry. The former follows, of course, the sequence of ionization potentials of the different charge states in the radial electron temperature gradient, the latter is a consequence of both the poloidally asymmetric C^0 source distribution with a maximum around the ALT-II limiter position and the magnetic field configuration. The poloidal asymmetry is, of course, especially pronounced for the lowest charge states, being populated by ionization rather than by transport processes, and gradually decreases with increasing charge state. Even for the highest charge states there still remain vertical (top-bottom) asymmetries and differences between high and low field side (along the midplane). The former are a neoclassical effect (with an ion accumulation for $z \geq 4$ at the top position under normal magnetic field direction as presupposed in the calculations), the latter are a consequence of the Shafranov shift of the magnetic surfaces (with a slight ion accumulation at the inboard position). The neoclassical effect is a result of a balance between the vertical (centrifugal and $\vec{\nabla}_{\perp}B$) drift and the $\|\vec{B}$ convection subject to friction and thermal forces. The latter are zero in the plasma core as a consequence of the assumption that ion/electron temperatures are constant on a magnetic flux surface. The up-down asymmetry becomes stronger with increasing collisionality as indicated by bolometric measurements. The Shafranov shift broadens the magnetic flux tubes in radial direction when passing from the low field side to the high field side, while keeping the area $2\pi R_0 h_\phi^* h_r dr$ almost constant, since $h_r h_\phi^* \simeq 1$. There is a concomitant increase of the radial gradient lengths decreasing both the radial diffusion and the poloidal drift velocity, but no change (up to terms of the order r^2/R_0^2) of the Pfirsch-Schlüter contribution to $|nV_{\|}|$ when comparing poloidal positions mirrored at $\theta = \pi/2$ or $\theta = 3\pi/2$.

The vertical and horizontal asymmetries are best seen from the corresponding 2D-plots in figs.5/6 and indirectly documented in the line integrated radiation profiles as shown in fig.7. The horizontal asymmetries are compared with experimental observations by the Li^0 beam activated cx spectroscopy of C^{z+} for $z \geq 4$ at the outboard midplane of the plasma. It is clearly seen that with consideration of the Shafranov shift of the magnetic surfaces the radial position of the density maxima is well reproduced, whereas the magnitude of the maxima is given within a factor of less than 1.5 using a coherent set of experimental plasma parameters. For the same parameters the line integrated radiation profiles are given within an angular range as seen by a spectrometer installed at an upper vessel position. In this case the numerical data show, however, some significant deviations from the measured signals. Apart from an abrupt disappearance of the calculated line integrals of the lower charge states ($z \leq 3$) at the high field side, there are differences in the angular asymmetry and the position of the radiation maxima of these states. As compared to calculations under sole consideration of the limiter source of C^0 (fig.7a), those with consideration of an additional uniform wall source of C^0 (fig.7b) lead to nearly symmetric angular profiles of C^{3+} (in contrast to experimental observations), but to the correct angular asymmetry in C^{2+}. Both calculations show a marked outward shift of the radiation maximum of C^{2+} near that of C^{3+} at the low field side, as compared to the experimental observations, but give a correct picture of the C^{4+} radiation signals. Like the bolometric measurements the line emission measurements clearly indicate the accumulation of lowly charged carbon (and oxygen) in the vicinity of the ALT-II limiter. It should be noted that the experimental values of the line integrated radiation profiles refer to selected line transitions for each considered charge state and to plasma conditions, which are probably different from those prevailing during the density measurements and used in these calculations. Moreover, since nearly all line transitions considered in the calculations start from the ground state, a comparison with the measured line transitions is only meaningful for C^{2+} and C^{4+}. For C^{3+}, however, a line transition between rather high principal quantum numbers has to be chosen for the UV-spectroscopy. Due to the different population channels for the initial state, the radiation of this line transition may follow a different electron temperature dependence than the radiation of line transitions from the ground state. The above mentioned discrepancies between the numerical and experimental data are therefore not surprising, also in view of the complete neglect of charge- exchange processes (at the plasma edge) and the uncertainties in the C^0 source distribution and the anomalous diffusion coefficient for the C^{z+} ions.

Another uncertainty concerns the boundary condition for the particle flux at the limiter surface (neglecting the real limiter shape and the corresponding influence on the impurity source distribution to be consistent with the geometry used in the SOLXY-code). In agreement with the chosen boundary conditions we always expect a density decrease towards the limiter surface with the build-up of density maxima in the poloidal C^{z+} profiles within the scrape-off layer as shown in fig.8. This follows from the requirement of a one-sided distribution function for each carbon charge state with no ion re-emission from the limiter surface. Since it presupposes that the particle flux onto the limiter is non-zero, it excludes particle flux reversal at some distance from the limiter. This may arise, if the poloidal components of both the electric drift and the thermoforce point away from the limiter (as usually is the case on the ion side of the limiter). Their effect on the poloidal impurity ion flow velocity inside the scrape-off layer may overcompensate the effect of the longitudinal electric and friction forces, which in the trace impurity limit are always directed towards the limiter. In such cases the pressure gradient of the carbon ion species under consideration is artificially increased to satisfy formally the boundary condition, which has lost its physical meaning. As a consequence slightly negative densities appear for C^{5+} and C^{6+} just in front of the ion side of the limiter. The same problem arises with a boundary condition, which prescribes (instead of the one-sided distribution function related to a particle flux onto the limiter surface) the poloidal velocity $V_\theta = V_\theta^E - \Theta h_\phi^*(V_\|^0 - D_\| \partial \ln n / \partial x_\|)$ as being always directed onto the limiter surface.

In the presently considered situation of carbon atom emission from the limiter head preferentially into the edge region inside the separatrix (the ionization length being much larger than the gyroradius under typical plasma edge conditions), the boundary conditions influence the poloidal density profiles in the scrape-off layer in accordance with the non-uniform carbon ion outflux across the separatrix, the non-uniformity being produced by the magnetic field configuration, in particular by the vertical drift, which due to the presence of the limiter cannot be short-circuited by a $\|\vec{B}$ motion (Pfirsch-Schlüter effect). This is to be contrasted with a situation, in which strong density gradients are built-up in front of the limiter by successive ionization of neutrals directly emitted from the limiter into the SOL (coupled with a high redeposition probability and necessitating a kinetic or Monte-Carlo calculation [8]). It should be noted that thermalization of lowly charged impurity ions with the background ions is seldom achieved in limiter tokamaks. If, however, the neutrals are predominantly sputtered into the region inside the separatrix, where ionization causes a fast transfer to higher charge states, a more efficient thermalization is possible, unless the increase of plasma density and impurity charge is overcompensated by a steep ion temperature increase.

Acknowledgement:

We greatly acknowledge the assistence of Mrs. B.Küppers from IPP and Mrs. R.Zimmermann from ZAM in the computer graphics.

References:

[1] R.P. Schorn et al., Appl. Phys. B 52, 71 (1991)
[2] G.Telesca et al., Nucl. Fusion 34(5), 625 (1994)
[3] J.Rapp, private communication
[4] H.A.Claaßen, H.Gerhauser, KFA-Report Jül-2576, Jan. 1992
[5] H.A.Claaßen et al., J.Nucl.Mat. 176/177, 398 (1990)
M.Z.Tokar, Plasma Phys. Control. Fusion 36, 1819 (1994)
[6] A.Rogister, Phys. Plasmas 1(3), 619 (1994)
[7] H.Gerhauser, H.A.Claaßen, J.Nucl.Mat. 176/177, 721 (1990)
[8] H.A.Claaßen, H.Repp, Nucl. Fusion 23(5), 597 (1983)
P.C.Stangeby, J.D.Elder, J.Nucl.Mat. 196/198, 258 (1992)
U.Kögler, J.Winter, H.G.Esser, to be presented at the
22th EPS Conf. on CFPP, Bournemouth/UK (1995)

Appendix I:

According to the changing importance of the various longitudinal ($\|\vec{B}$) forces, the estimates for $\tau_{\|}$ are given separately for the regions inside and outside the separatrix:

plasma periphery inside the separatrix:

The $\|\vec{B}$ momentum of the lower charge states appearing as a result of electron impact ionization of neutrals emitted preferentially from the limiter head into the region inside the separatrix, is essentially governed by a balance between inertial, friction (with the background hydrogen ions in the limit $V_{\|+} \simeq 0$), and pressure forces as well as momentum transfer during ionization. Using the approximations $\nabla_{\|}(kT_{+,-}, \Phi) \simeq 0$ and $(\nu_I n)_z \simeq (\nu_I n)_{z-1} \simeq Q_0$, we obtain (omitting again the index z):

$$(\alpha\nu_C + \nu_I + \nabla_\| V_\|)V_\| = \nu_I V_{\|,z-1} - \frac{kT}{M}\nabla_\| \ln n \quad \text{with} \quad \nabla_\| \ln n \simeq \nabla_\| \ln Q_0$$

because $\nabla_\| \nu_I \simeq 0$ in accordance with the neglect of thermoforces. For $\nabla_\| \simeq -\Theta\partial/(a\partial\theta)$ at $r \simeq a$ (ignoring the θ-dependence of h_ϕ^*), the ansatz

$$Q_0 \sim \exp\Big[-\frac{a^2(\theta - \theta_L^*)^2}{\lambda^2}\Big] \quad \text{with} \quad V_{\|,z=0} = 0$$

suggests the solution $V_\| = -a(\theta - \theta_L^*)/(\Theta\tau_\|)$ leading to the recursion formula

$$\frac{1}{\tau_\|} = -\frac{1}{2}(\alpha\nu_C + \nu_I) + \sqrt{\frac{1}{4}(\alpha\nu_C + \nu_I)^2 + \Big(\frac{\Theta v_T}{\lambda}\Big)^2 + \frac{\nu_I}{\tau_{\|,z-1}}}$$

where $v_T^2 = 2kT/M$.

In particular, for $z = 1$ and $\nu_I \gg \alpha\nu_C$ we would get the relation

$$\frac{2}{\nu_I\tau_\|} \simeq \sqrt{1 + \Big(\frac{2\Theta v_T}{\lambda\nu_I}\Big)^2} - 1$$

where $\nu_I\tau_\| \to \infty$ for either $\nu_I \to \infty$ or $\lambda \to \infty$, and

$$\Gamma_\| = -Q_0(\theta_L^*)\frac{a(\theta - \theta_L^*)}{\Theta\nu_I\tau_\|}\exp\Big[-\frac{a^2}{\lambda^2}(\theta - \theta_L^*)^2\Big] \to 0 \quad \text{for} \quad \frac{a(\theta - \theta_L^*)}{\lambda} \to \infty$$

which, of course, holds for all z. In the numerical calculations we used the approximation $V_{\|,z=1} = 0 = 1/\tau_{\|,z=1}$. For higher charge states, where $\nu_I \ll \alpha\nu_C$, we would obtain

$$\frac{2}{\alpha\nu_C\tau_{\|}} \simeq \sqrt{1 + \left(\frac{2\Theta v_T}{\lambda\alpha\nu_C}\right)^2} - 1$$

<u>scrape-off layer:</u>

Neglecting, in a rough approximation, thermal and pressure forces, we obtain

$$(\alpha\nu_C + \nu_I + \nabla_{\|}V_{\|})V_{\|} = \nu_I V_{\|,z-1} + \alpha\nu_C V_{\|+} + \frac{zeE_{\|}}{M}$$

Setting $E_{\|} = -E_{\|L}[\theta - (\theta_L + \pi)]/\pi$ with $E_{\|L} = \Theta kT_-/e\pi a$ and $V_{\|+} = -c_s[\theta - (\theta_L + \pi)]/\pi$ with $c_s = \sqrt{2kT_-/m_+}$, we make the ansatz

$$V_{\|} = -\frac{a[\theta - (\theta_L + \pi)]}{\Theta\tau_{\|}}$$

which leads to the recursion formula

$$\frac{1}{\tau_{\|}} = -\frac{1}{2}(\alpha\nu_C + \nu_I) + \sqrt{\frac{1}{4}(\alpha\nu_C + \nu_I)^2 + \alpha\nu_C\nu_s + \frac{zm_+\nu_s^2}{2M} + \frac{\nu_I}{\tau_{\|,z-1}}}$$

where $\nu_s \equiv \Theta c_s/\pi a$. Note that $a/\Theta = q_a R_0$, where q_a is the safety factor at $r = a$. It follows from the ansatz for $E_{\|}$ that the electrostatic potential in front of the limiter is $\Phi_L = -(1/2)(kT_-/e)$ as compared to $\Phi_L = -(\ln 2)(kT_-/e)$ when assuming a Boltzmann relation for the electrons with a density ratio of 0.5 between limiter position and stagnation point. For charge states, which in the scrape- off layer satisfy $\alpha\nu_C \gg \nu_I$ we get the approximate formula

$$\frac{1}{\tau_{||}} \simeq \frac{\alpha\nu_C}{2}\Big[\sqrt{1+\frac{4\nu_s}{\alpha\nu_C}+\frac{zm_+}{8M}\Big(\frac{4\nu_s}{\alpha\nu_C}\Big)^2}-1\Big]$$

with the limiting values of either $1/\tau_{||} \simeq \sqrt{\alpha\nu_C\nu_s}$ for the friction force dominated case $\alpha\nu_C \gg 4\nu_s$ or $1/\tau_{||} \simeq \nu_s\sqrt{zm_+/2M}$ for the electric force dominated situation, where $\alpha\nu_C \ll zm_+\nu_s/2M$.

AppendixII:

In case of complete neutralization the distribution function of an ion species becomes one-sided in front of a target. The representation of the ion distribution function as a series expansion into polynomials, which are orthogonal over the whole velocity space, therefore requires a large number of expansion coefficients (depending on the choice of the weight function) and a kinetic treatment of the presheath region (between the fluid region and the Debye sheath) in order to get a satisfactory approximation of the real situation. In a crude approximation, however, the presheath region, in which the weakly disturbed shifted Maxwellian of the fluid region passes into the strongly disturbed one-sided distribution function in front of the target, may be bridged by the assumption of particle, momentum, energy etc. flux conservation (i.e. neglecting particle, momentum and energy sources in this region irrespective of inelastic collision processes and electric field effects). The constraints of the distribution function in front of the target may then be translated into boundary conditions for the fluid region (this method has a long tradition and is mainly used for the majority ion species in context with Bohm's criterion). Since in the trace impurity limit under consideration Bohm's criterion does not imply any constraints on the distribution function of the impurity ions, the boundary conditions for the corresponding series expansion coefficients may be directly derived from the neutralization condition at the target. This is done here by considering a series expansion of the impurity ion (guiding-centre) distribution function in Hermitian polynomials with a shifted Maxwellian as weight function. In a very crude approximation we take only the first two expansion coefficients into account and construct a relation between them from the condition that the particle flux over the corresponding velocity half-space should vanish (a generalization of this method to include a larger number of expansion coefficients and attributed flux relations is straightforward). In order to get a relation for the particle flux component perpendicular to the wall in the presence of an oblique magnetic field, we have to incorporate in the boundary condition the poloidal component of the electric drift. Whereas the latter keeps its sign, the normal to the target surface changes its sign when going from the electron side to the ion side of the limiter.

With the ansatz

$$f(v_{\|}) = \sum_{m=0}^{1} \frac{A_m}{v_T^{m+1}\sqrt{\pi}} H_m(\xi) \exp(-\xi^2) \quad \text{with} \quad \xi = \frac{v_{\|} - V_{\|}^0}{v_T}$$

the particle density and parallel particle flux density are

$$n = \int_{-\infty}^{+\infty} f(v_{\|}) dv_{\|} = A_0 \quad \text{and}$$

$$\Gamma_{\|} = \int_{-\infty}^{+\infty} v_{\|} f(v_{\|}) dv_{\|} = V_{\|}^0 A_0 + A_1 = V_{\|}^0 n - D_{\|} \nabla_{\|} n$$

From the conditions $\int_{-\infty}^{0} dv_\theta v_\theta f(v_{\|}) = 0$ resp. $\int_{0}^{+\infty} dv_\theta v_\theta f(v_{\|}) = 0$ with $v_\theta = -(E_r/B + \Theta h_\phi^* v_{\|})$ we derive the relations

$$A_0 v_T g + A_1 = \mp \frac{\exp(-g^2)}{\sqrt{\pi}(1 \pm \text{erf} g)} A_0 v_T \quad ; \qquad g \equiv \frac{1}{v_T}\Big(\frac{E_r}{\Theta B_0} + V_{\|}^0\Big)$$

for the ion side (upper sign) resp. electron side (lower sign) of the limiter. These relations between A_0 and A_1 constitute on each side of the limiter a boundary condition for the particle balance equation coupling the density n with its gradient $\nabla_{\|} n$.

Figure captions:

fig.1 : (ξ, η)-physical plane showing the minor TEXTOR cross section with ALT-II limiter position and projections of Shafranov-shifted magnetic flux surfaces labelled by $r = const.$ forming nearly excentric circles with Cartesian coordinates $\xi = rh_\theta^* \cos\theta + h_r(a-r)^2/(2R_0)$ and $\eta = rh_\theta^* \sin\theta$. Note the curved lines $\theta = const.$

fig.2 : triangulation and boundary conditions in the (x, y)- calculation plane, in which the projections of the Shafranov- shifted magnetic flux surfaces appear as concentric circles $(x, y) = r(\cos\theta^*, \sin\theta^*)$. For the poloidal shift $\theta^* = \theta + \pi/4$, the ALT-II limiter is symmetrically intersected by the x- axis.

fig.3 : functions $F^{\pm}(g)$ determining the $\|\vec{B}$ density gradients at the ion/electron $(+/-)$ side of the toroidal belt limiter:

$$\frac{\partial \ln n}{\partial x_{\|}}|_{\pm} = \frac{v_T F^{\pm}(g)}{D_{\|}} \quad ; \quad F^{\pm}(g) = g \pm \frac{\exp(-g^2)}{\sqrt{\pi}(1 \pm \mathrm{erf} g)} \quad ; \quad g = \frac{\Theta V_{\|}^0 - V_\theta^E}{\Theta v_T}$$

fig.4 : density (4a) and line radiation (4b) distribution of C^{z+} (with $2 \leq z \leq 6$ for the density and $2 \leq z \leq 5$ for the line radiation) over the minor cross section of TEXTOR in a given deuterium plasma (4c) assuming a Gaussian line source of C^+ along the separatrix with $0.14m$ half-width and a maximum C^0 radial flux density of $2.33 * 10^{19}/(m^2 s)$ located poloidally near the limiter e-side. Note that the density of C^+ (4c) and the corresponding part in the total line radiation is calculated on the assumption of an ionization equilibrium $(n\nu_I)_1 = Q_0$.

fig.5 : 2D plots showing the asymmetries of the calculated $C^{z+}(2 \leq z \leq 6)$ density distribution (5a) along the horizontal line $\eta = 0$ ($\xi - axis$). They are compared with radial density profiles of the higher charge states $z \geq 4$ of carbon (5c) as measured along the outboard midplane by Li^0 beam activated cx-spectroscopy (5b).

fig.6 : 2D plots showing the asymmetries of the calculated $C^{z+}(2 \leq z \leq 6)$ density distribution (5a) along a nearly vertical line through the magnetic axis $\xi = a^2/2R_0 \quad \eta = 0$.

fig.7 : line-integrated radiation intensities (without and with a C^0-wall source $\rightarrow$ 7a,b) of the various ionization levels $C^{z+}(2 \leq z \leq 5)$ as a function of the angle α, for which the radiation would be seen from a spectrometer installed at the upper half of the TEXTOR vessel (7c). This is to be compared with the measured emissivities of selected lines of C^{2+} to C^{4+} (7d).

fig.8 : Z_{eff} and poloidal density profiles of $C^{z+}(2 \leq z \leq 6)$ inside the scrape-off layer at $r = 0.465m$ in accordance with the non-uniform particle flux across the separatrix and the boundary conditions, which force the densities to drop towards the limiter surface and to steepen their gradients at the i-side with increasing z. Note that the density of C^+ is calculated on the assumption of an ionization equilibrium $(n\nu_I)_1 = Q_0$. It is therefore not subjected to the boundary conditions of the differential equations, but merely follows the C^0-source distribution.

Minor TEXTOR cross section with ALT-II limiter

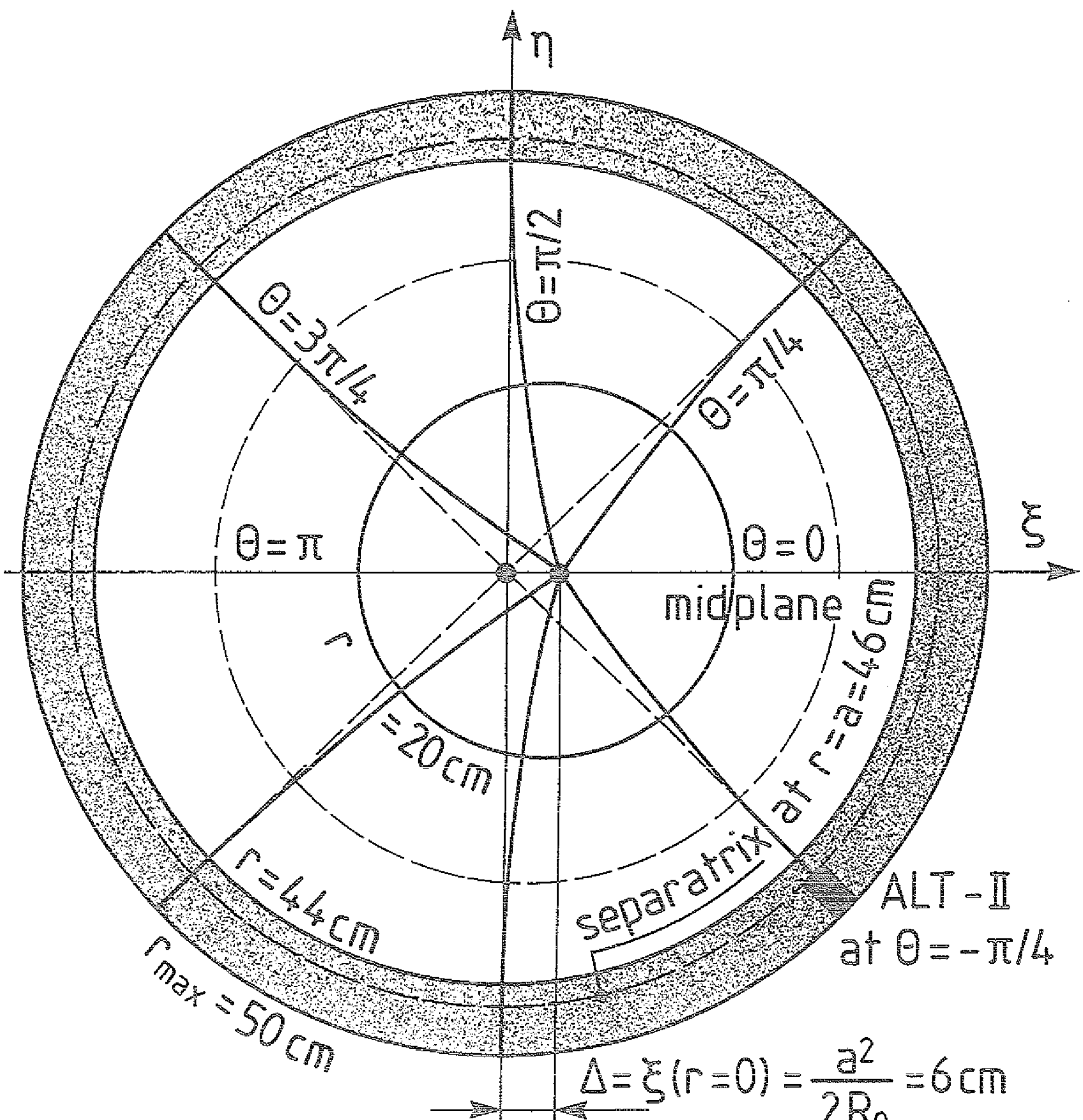

Shafranov-shifted magnetic flux surfaces r = const. forming nearly excentric circles with the Cartesian coordinates $\xi = r h_\theta^* \cos\theta + h_r (a-r)^2/(2R_o)$, $\eta = r h_\theta^* \sin\theta$

KFA Jülich IPP	**fig.1**	Gerhauser 1995
		67-6186

fig.2 boundary conditions:

e-side: $\Gamma_\theta = -\gamma^- n v_T$ i-side: $\Gamma_\theta = +\gamma^+ n v_T$ limiter head: $\Gamma_r = 0$

$$\gamma^\pm = \frac{\Theta \exp(-g^2)}{\sqrt{\pi}(1 \pm \mathrm{erf} g)} \quad , \quad g \equiv \frac{\Theta V_\parallel^0 - V_\theta^E}{\Theta v_T} \quad , \quad \text{liner wall at } r_w : n = 0$$

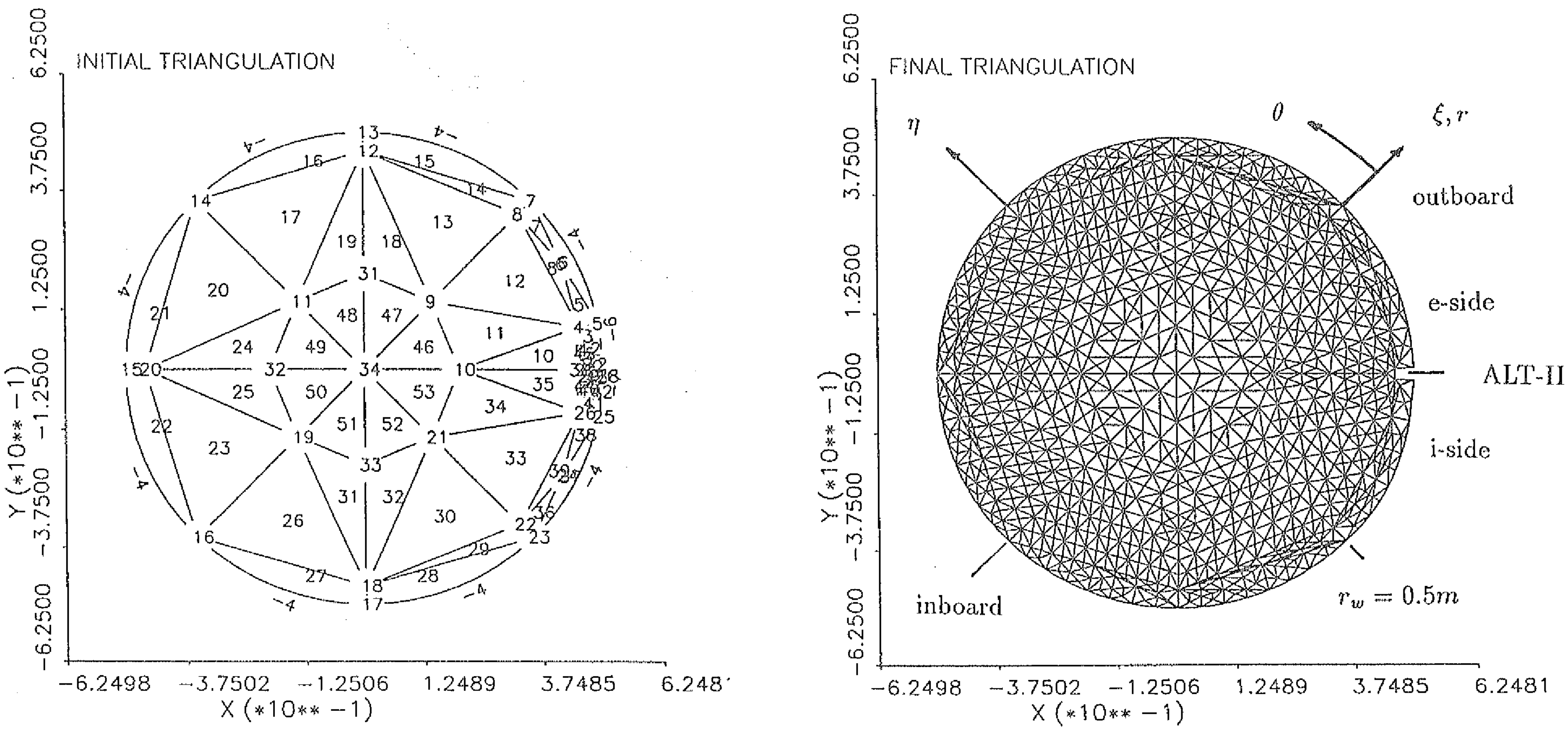

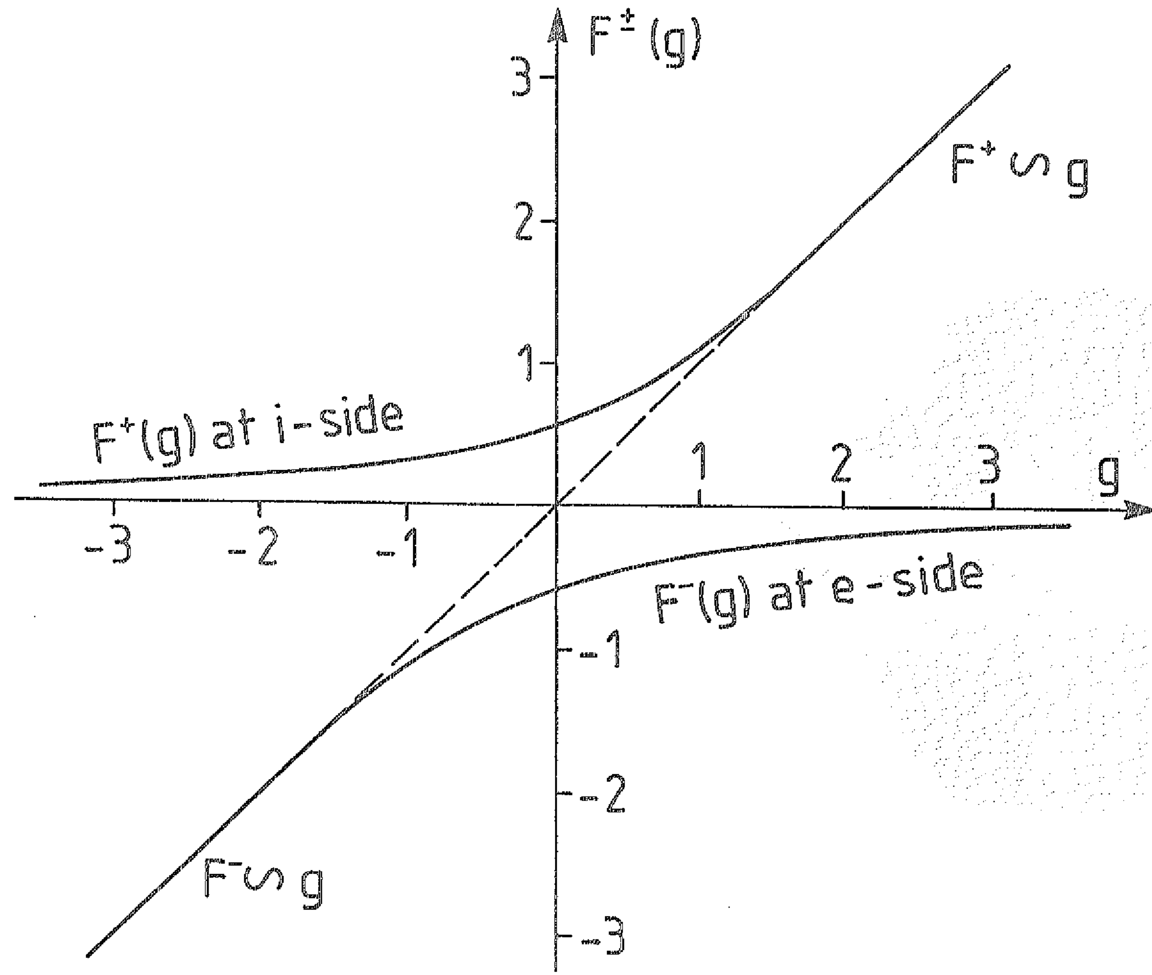

Jülich IPP

fig.3

$F^{\pm}(g)$ determining the $\|\vec{B}$ density gradient at the e/i (+/-) side of ALT-II

$$\frac{\partial \ln n}{\partial x_{\|}}\Big|_{\pm} = \frac{v_T F^{\pm}(g)}{D_{\|}} \quad ; \quad F^{\pm}(g) = g \pm \frac{\exp(-g^2)}{\sqrt{\pi}(1 \pm \mathrm{erf} g)} \quad ; \quad g = \frac{\Theta V_{\|}^{0} - V_{0}^{E}}{\Theta v_T}$$

Gerhauser 1995

67-6185

fig.4a

Calculated particle density distribution of

C^{z+} $(2 \leq z \leq 6)$

over the minor cross section of TEXTOR

$xi - min = -0.509$ $xi - max = 0.487$

$eta - min = -0.497$ $eta - max = 0.496$

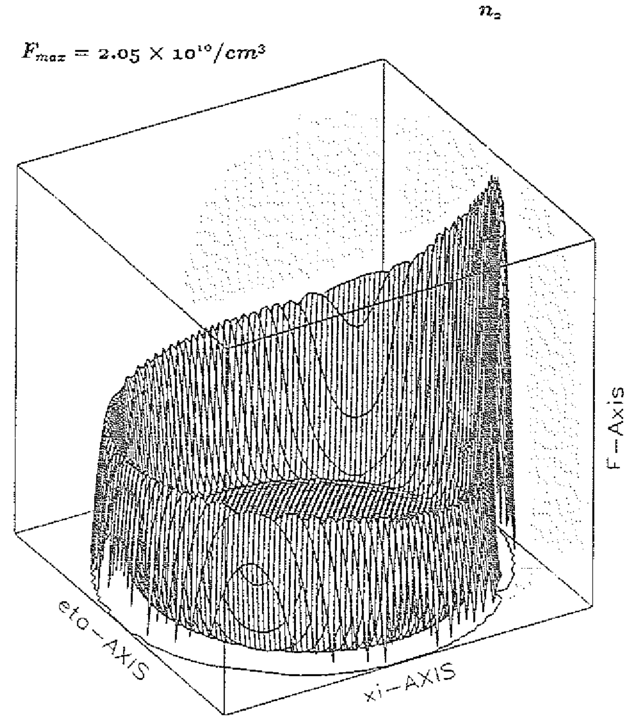

fig.4b

Calculated total line radiation profiles of

C^{z+} $(2 \leq z \leq 5)$

over the minor cross section of TEXTOR

$xi - min = -0.509$ $xi - max = 0.487$

$eta - min = -0.497$ $eta - max = 0.496$

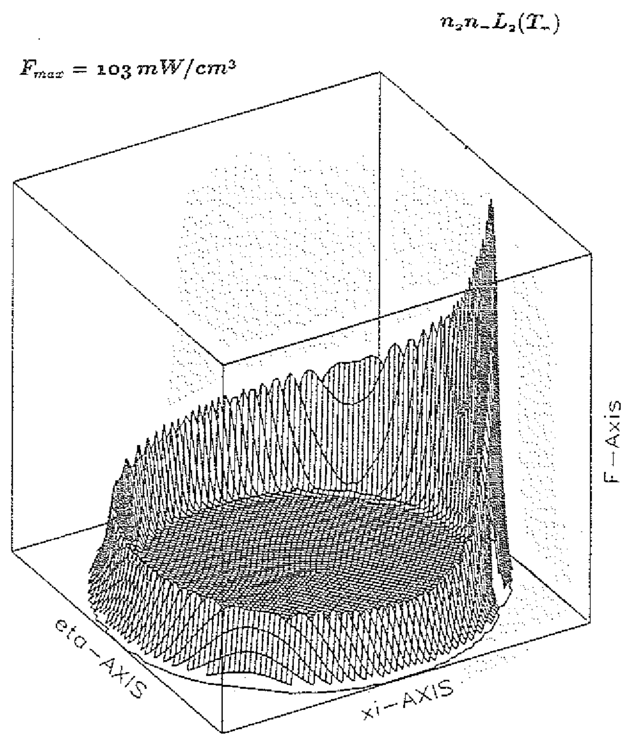

n_3

$F_{max} = 2.70 \times 10^{10}/cm^3$

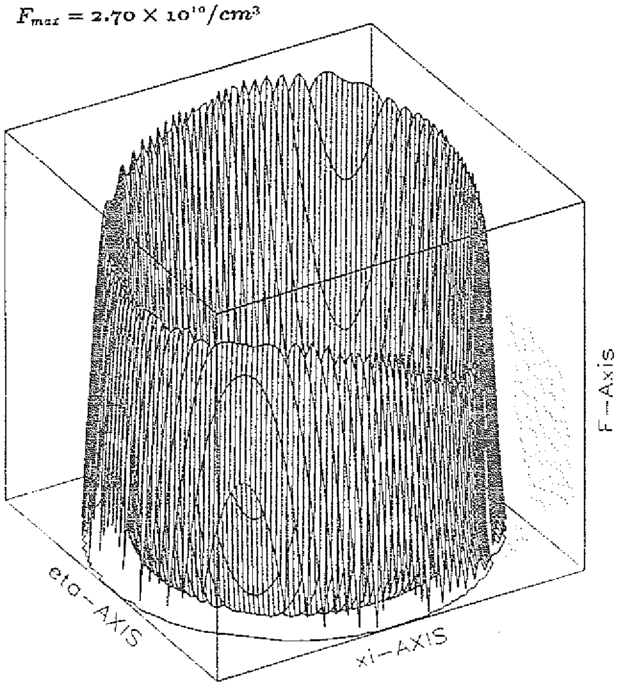

n_4

$F_{max} = 2.09 \times 10^{11}/cm^3$

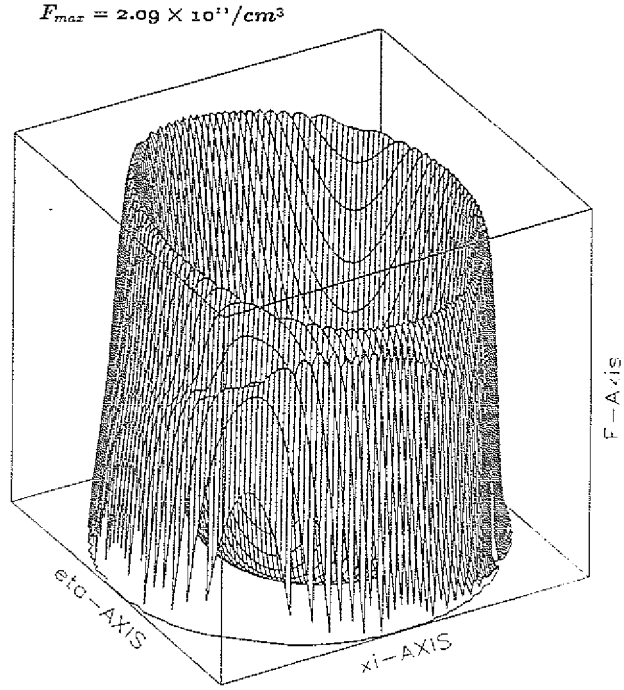

$n_3 n_- L_3(T_-)$

$F_{max} = 86.1\, mW/cm^3$

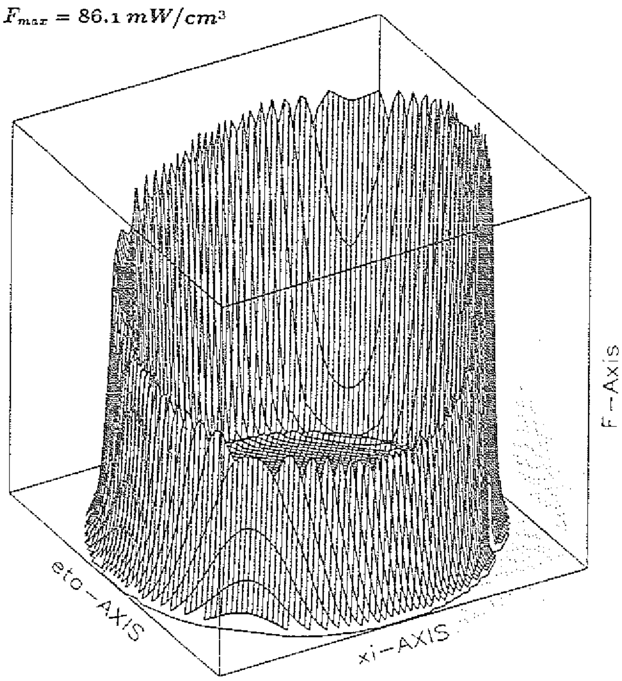

$n_4 n_- L_4(T_-)$

$F_{max} = 19.7\, mW/cm^3$

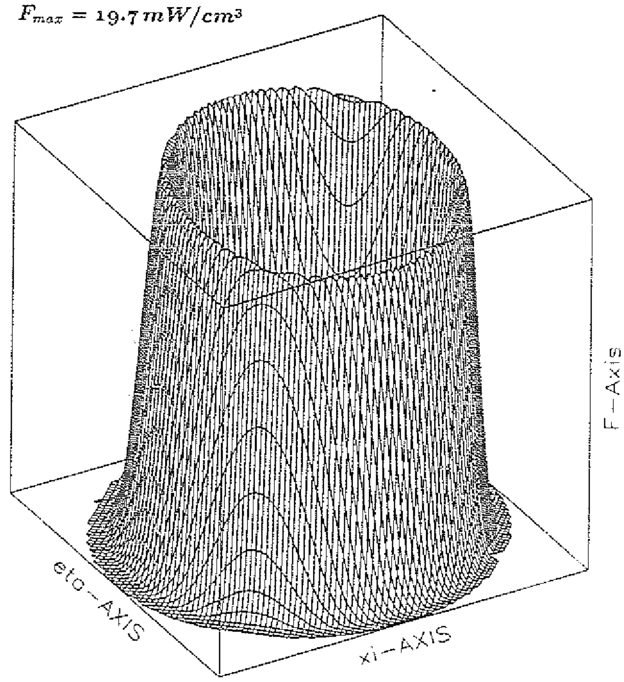

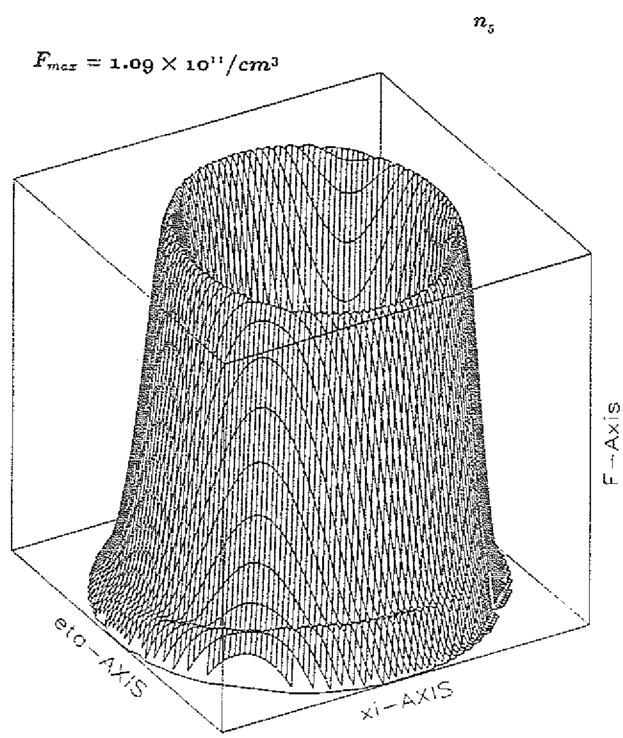

n_5
$F_{max} = 1.09 \times 10^{11}/cm^3$
F-Axis
eta-AXIS
xi-AXIS

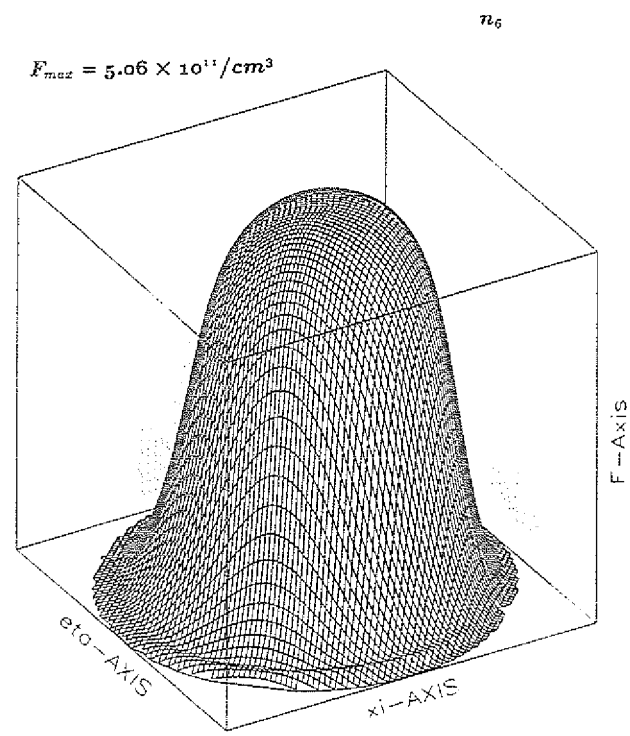

n_6
$F_{max} = 5.06 \times 10^{11}/cm^3$
F-Axis
eta-AXIS
xi-AXIS

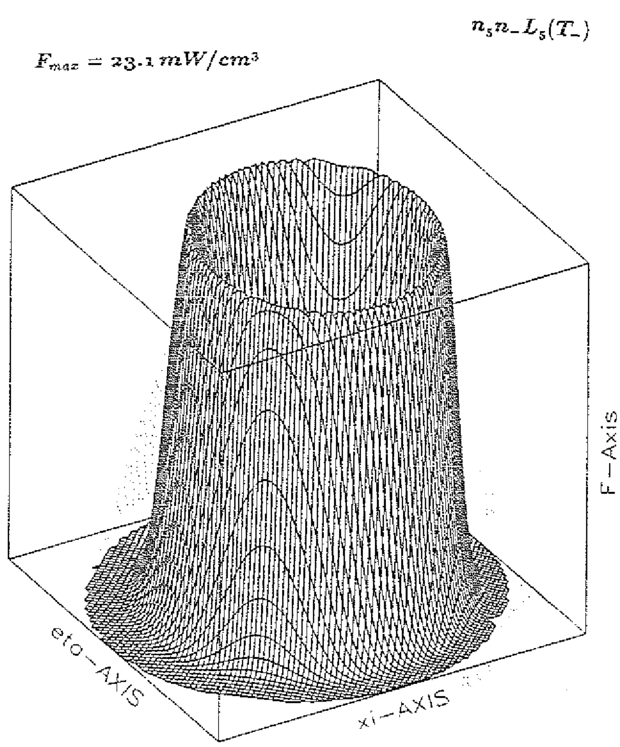

$n_5 n_- L_5(T_-)$
$F_{max} = 23.1\, mW/cm^3$
F-Axis
eta-AXIS
xi-AXIS

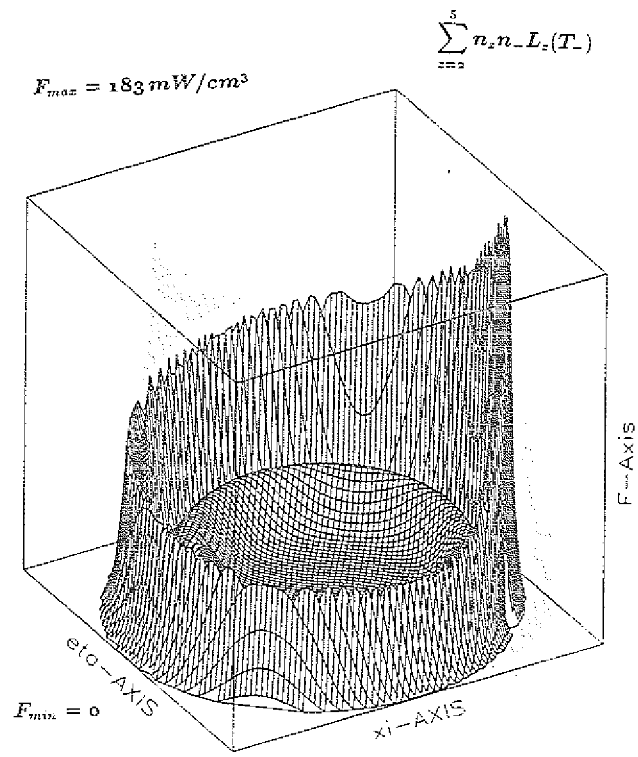

$\sum_{z=2}^{5} n_z n_- L_z(T_-)$
$F_{max} = 183\, mW/cm^3$
F-Axis
eta-AXIS
xi-AXIS
$F_{min} = 0$

$n_1 = Q_0/\nu_{I_1}$

$F_{max} = 2.30 \times 10^{10}/cm^3$

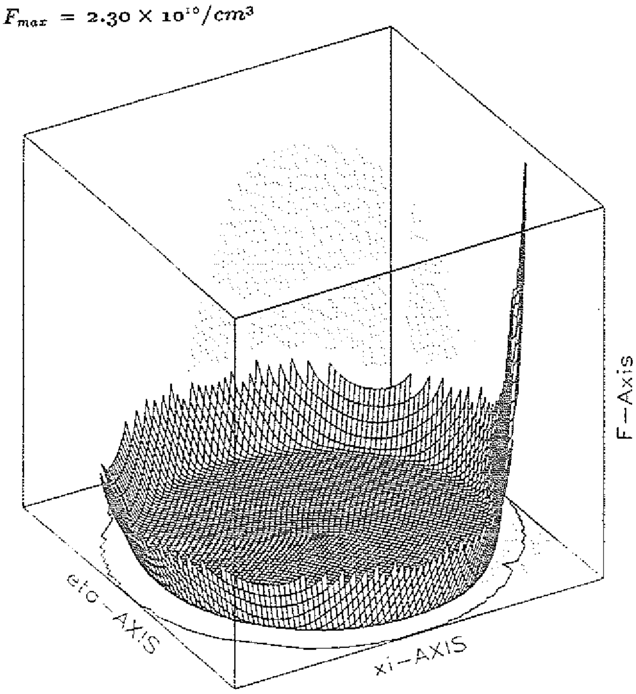

fig.4c

particle density of C^+ and total line radiation of $C^{z+}\,(1 \leq z \leq 5)$ assuming the ionization equilibrium $(n\nu_I)_1 = Q_0$ and prescribing the background plasma (shown example: electron density n_-)

$F_{max} = 213\, mW/cm^3$

$\sum_{z=1}^{5} n_z n_- L_z(T_-)$

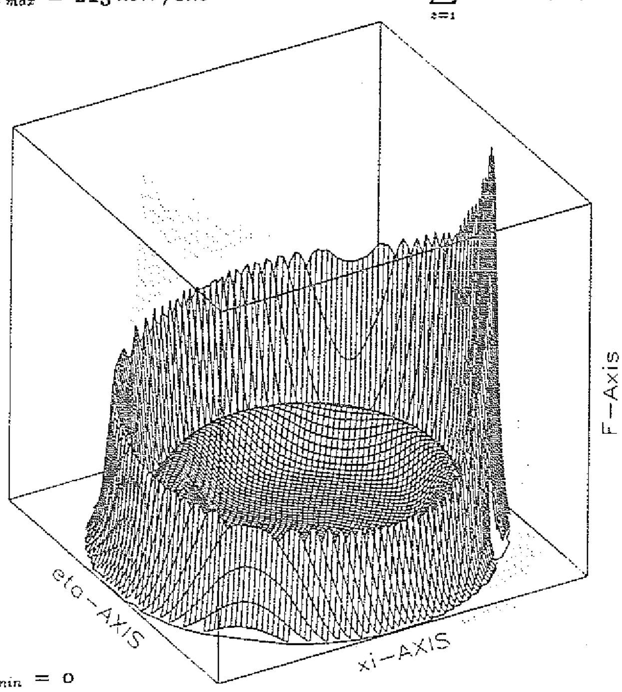

$F_{min} = 0$

n_-

$F_{max} = 3.30 \times 10^{13}/cm^3$

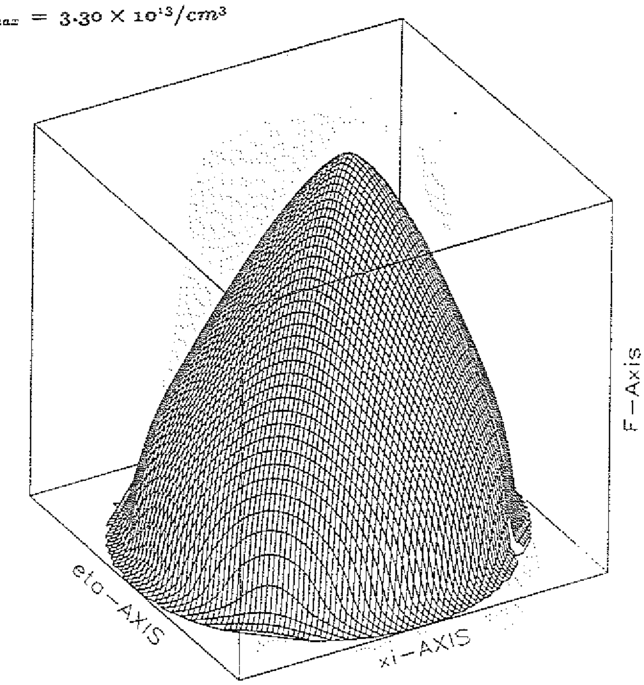

$F_{min} = 1.74 \times 10^{11}/cm^3$

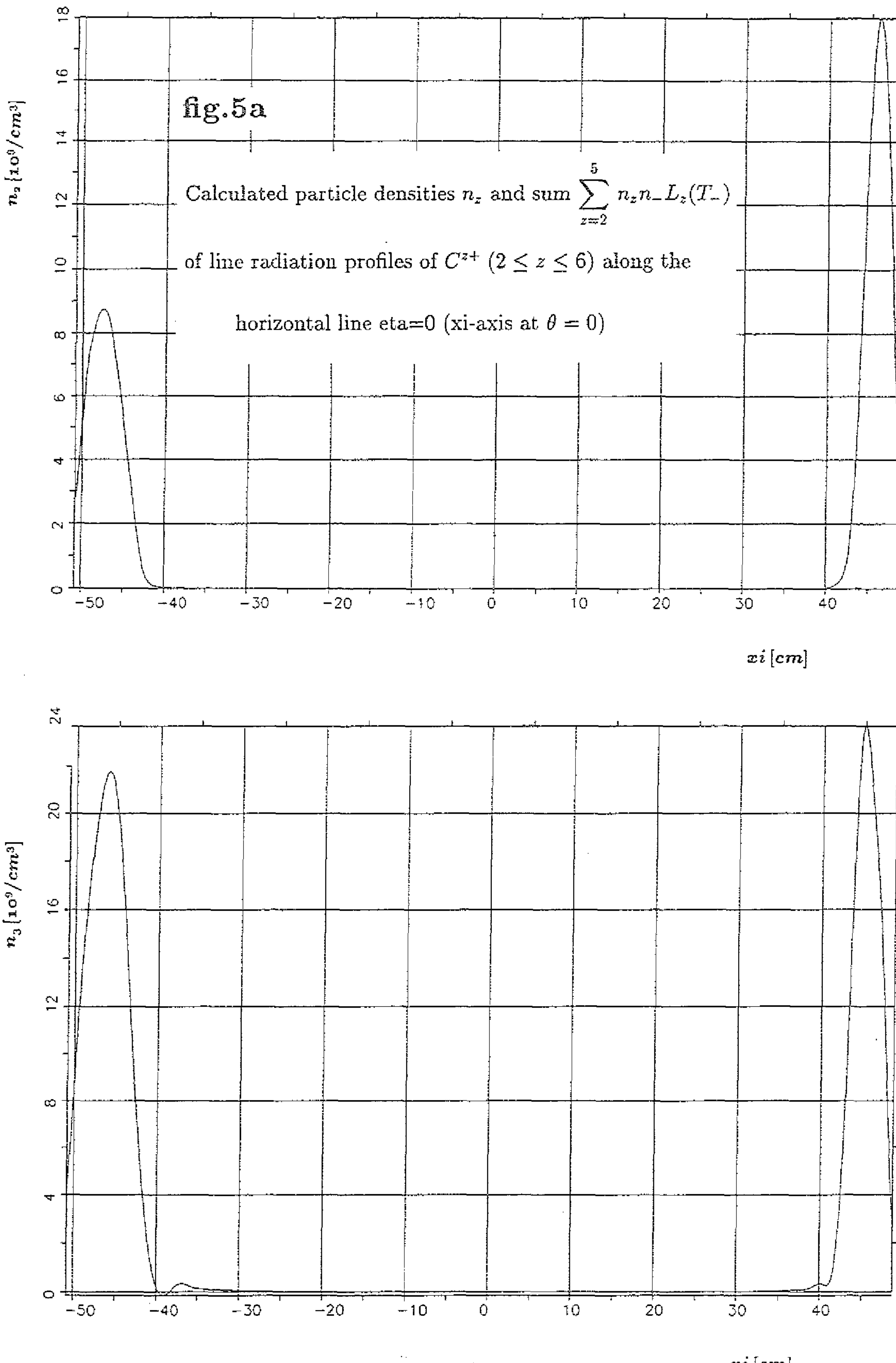

fig.5a

Calculated particle densities n_z and sum $\sum_{z=2}^{5} n_z n_- L_z(T_-)$ of line radiation profiles of C^{z+} $(2 \leq z \leq 6)$ along the horizontal line eta=0 (xi-axis at $\theta = 0$)

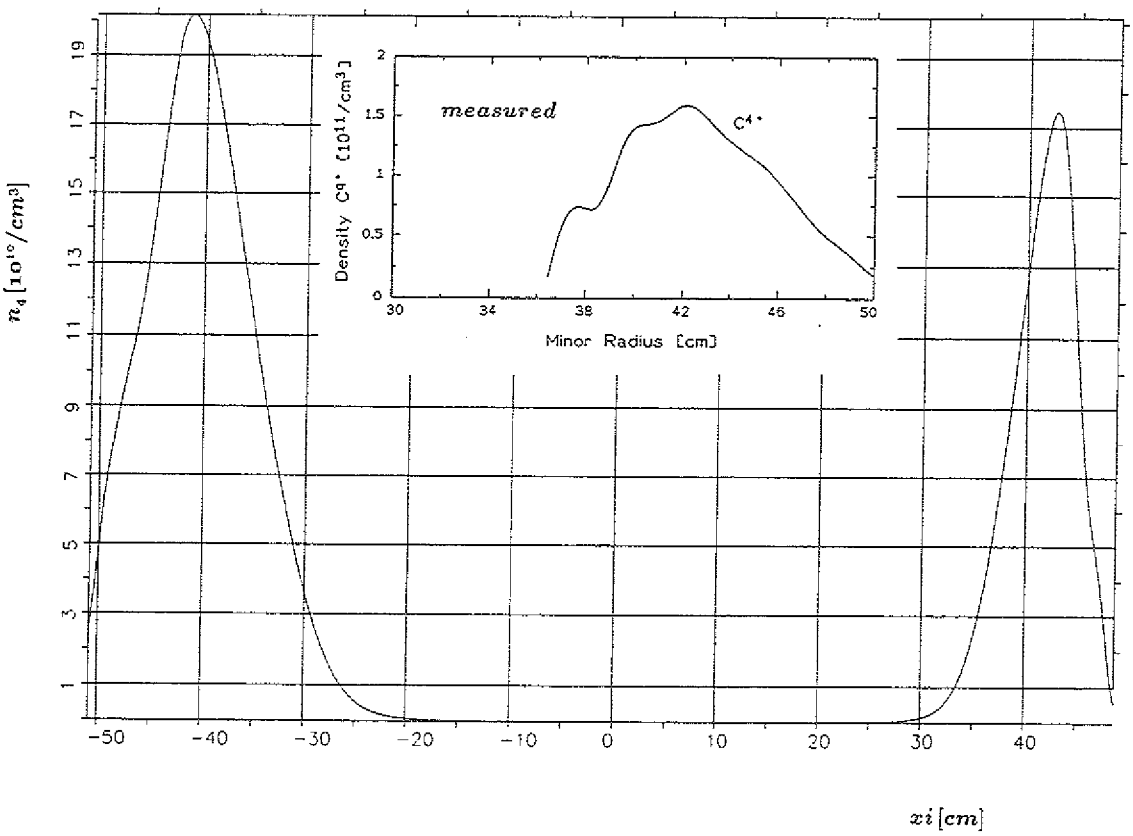

$n_4\,[10^{10}/cm^3]$
measured
C^{4+}
Density C^{q+} [$10^{11}/cm^3$]
Minor Radius [cm]
$xi\,[cm]$

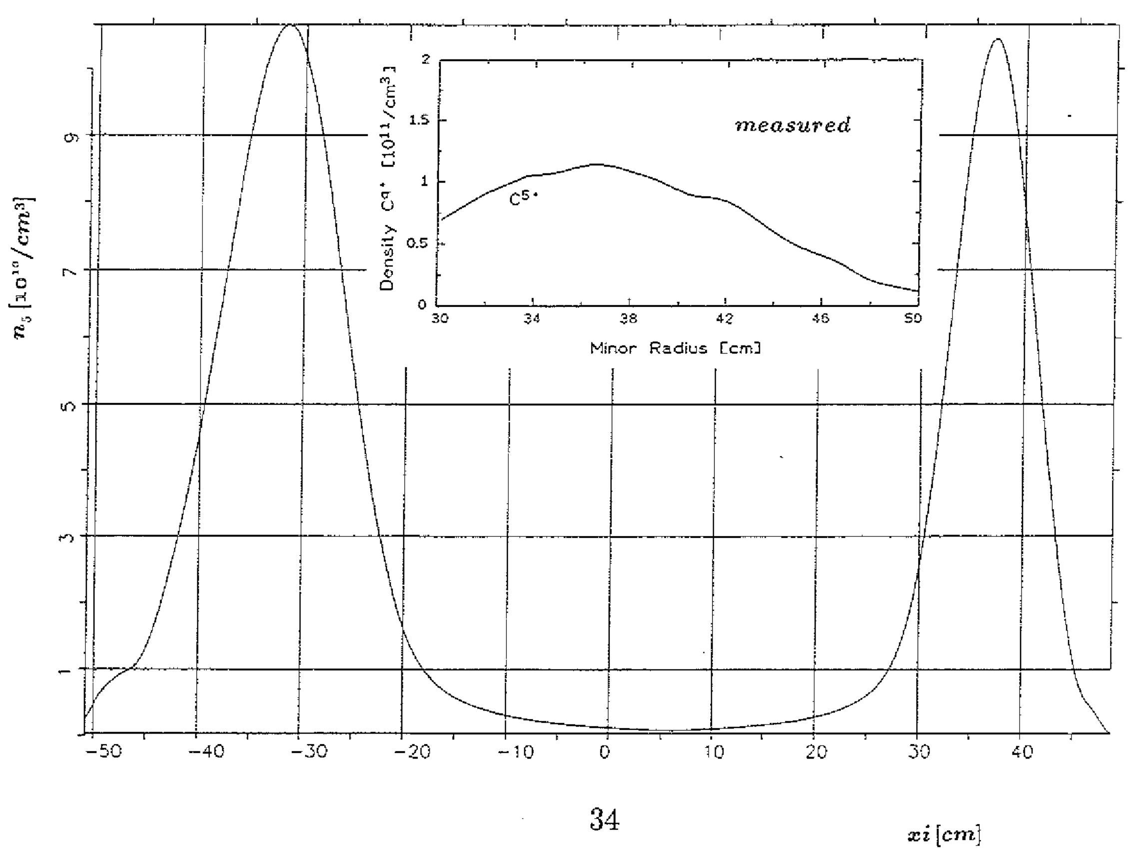

$n_5\,[10^{10}/cm^3]$
measured
C^{5+}
Density C^{q+} [$10^{11}/cm^3$]
Minor Radius [cm]
$xi\,[cm]$

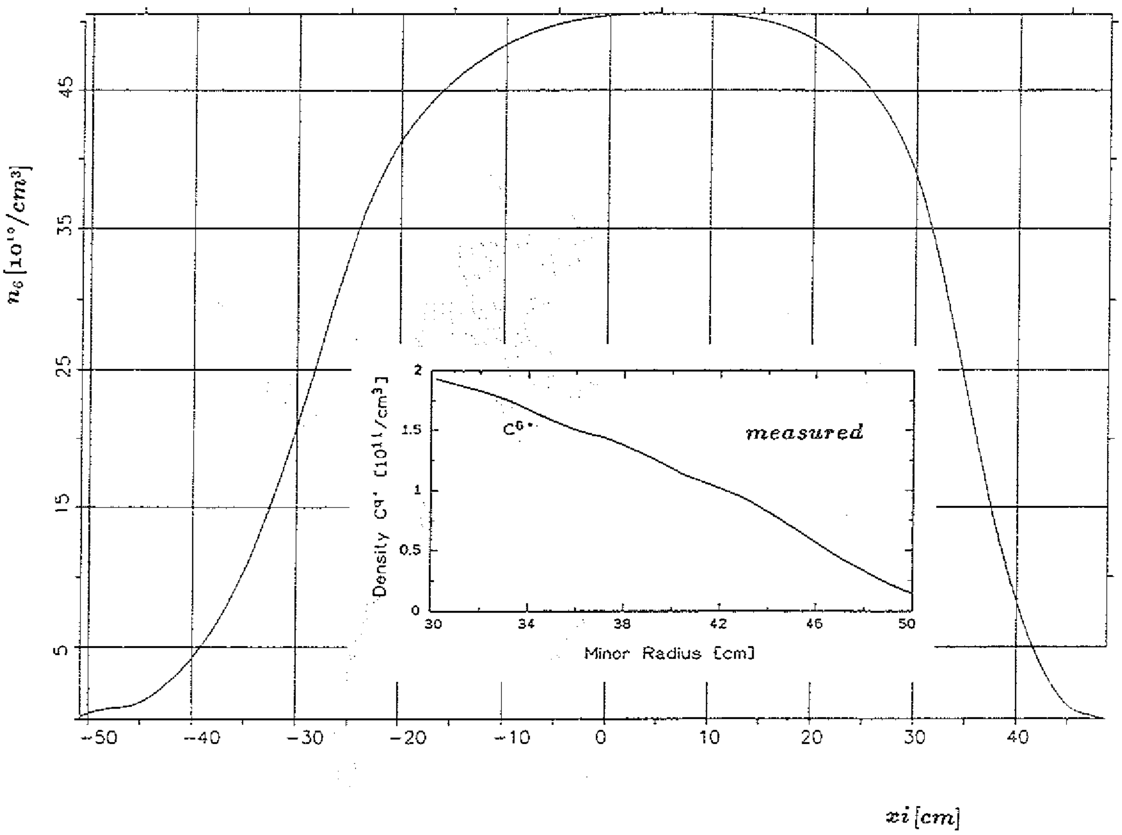

$n_6\,[10^{10}/cm^3]$
45
35
25
15
5
-50
-40
-30
-20
-10
0
10
20
30
40
$xi\,[cm]$
Density C6+ [10^11/cm^3]
C6+
measured
Minor Radius [cm]

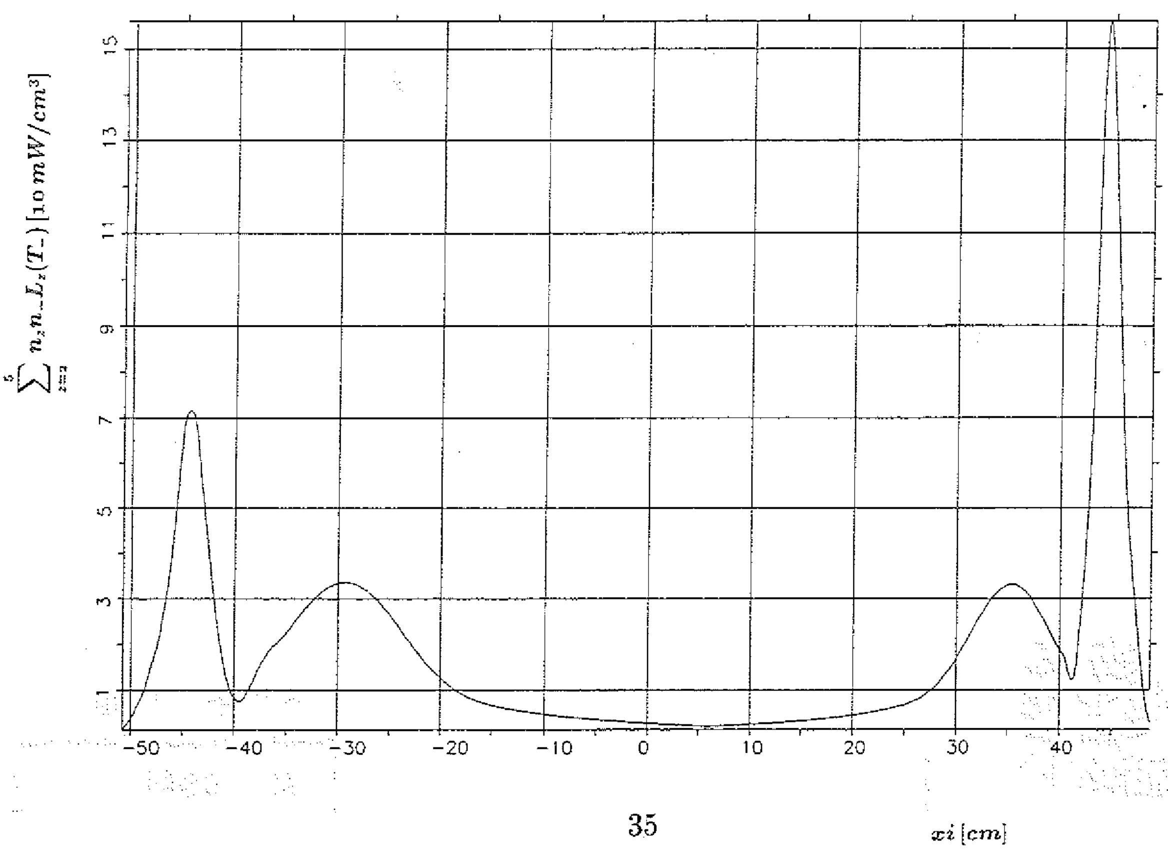

$\sum_{z=2}^{5} n_z n_- L_z(T_-)\,[1.0\,mW/cm^3]$
15
13
11
9
7
5
3
1
-50
-40
-30
-20
-10
0
10
20
30
40
$xi\,[cm]$

Experimental set-up for Li^0- beam activated cx-spectroscopy

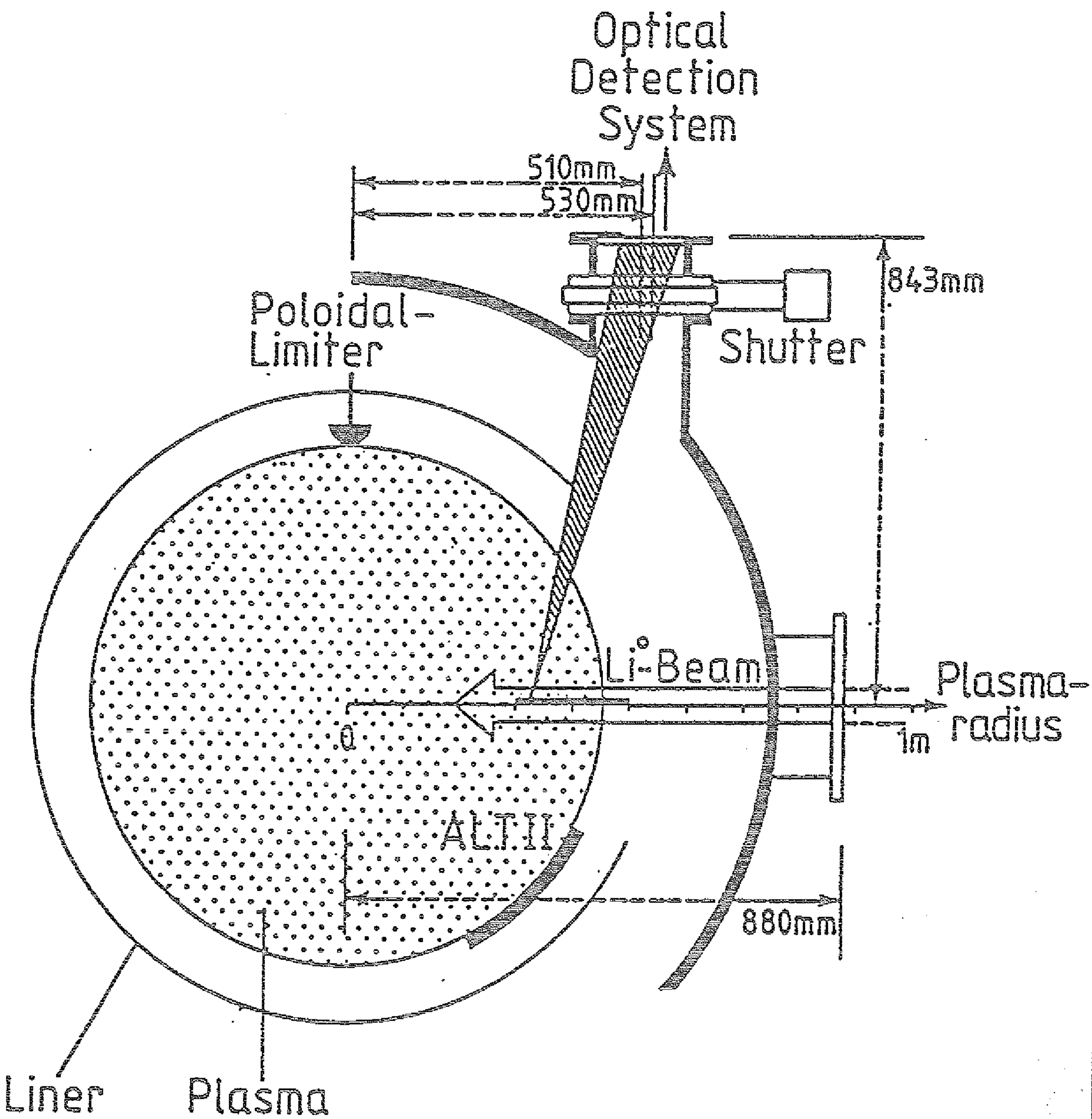

$$C^{z+} + Li^0 \rightarrow C^{(z-1)+} + Li^+ + h\nu$$

Jülich IPP

fig.5b

Schorn 1990

67 - 4851

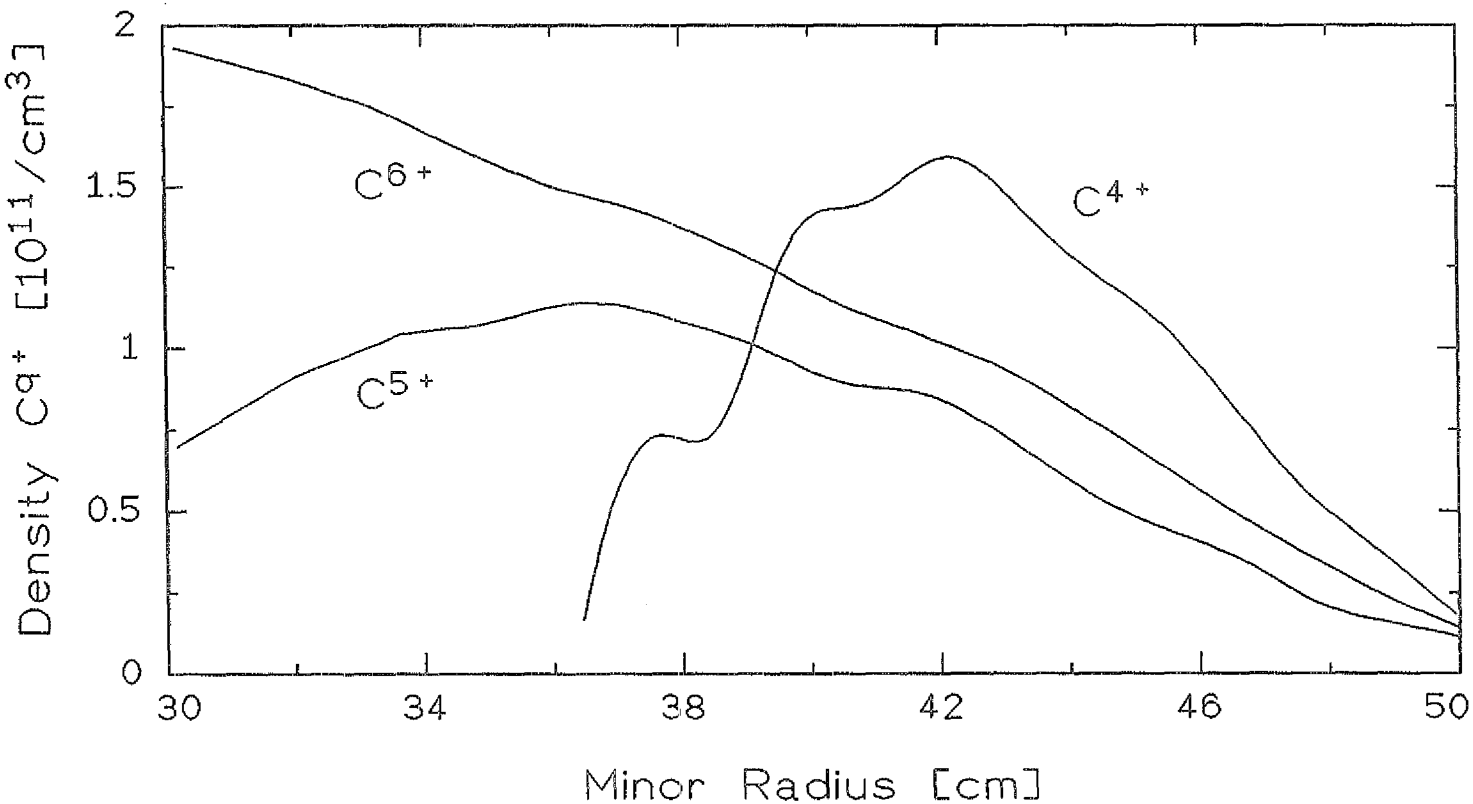

fig.5c **measured particle densities n_z of C^{z+} ($4 \leq z \leq 6$) along the horizontal line eta=0 (xi-axis at $\theta = 0$)**

fig.6

Calculated particle densities n_z and sum $\sum_{z=2}^{5} n_z n_- L_z(T_-)$ of line radiation profiles of C^{z+} $(2 \leq z \leq 6)$ along a nearly vertical line through the magnetic axis xi$=a^2/2R_0$, eta=0

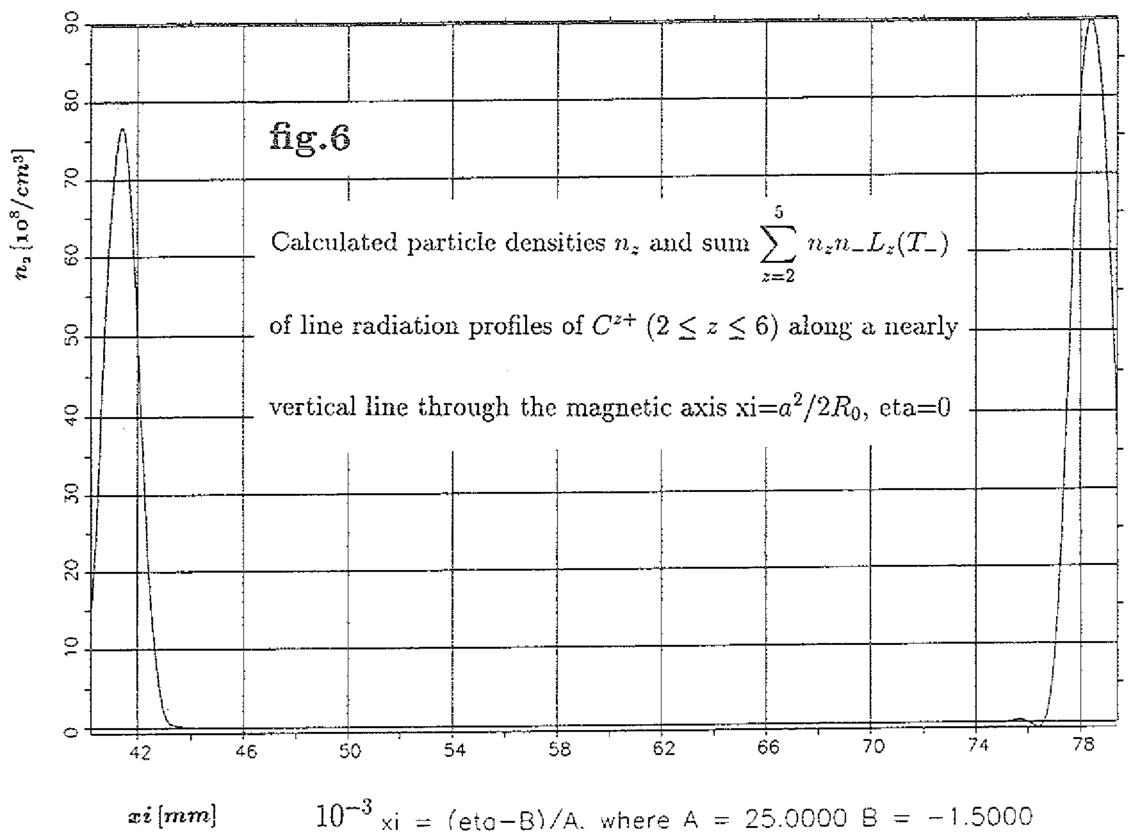

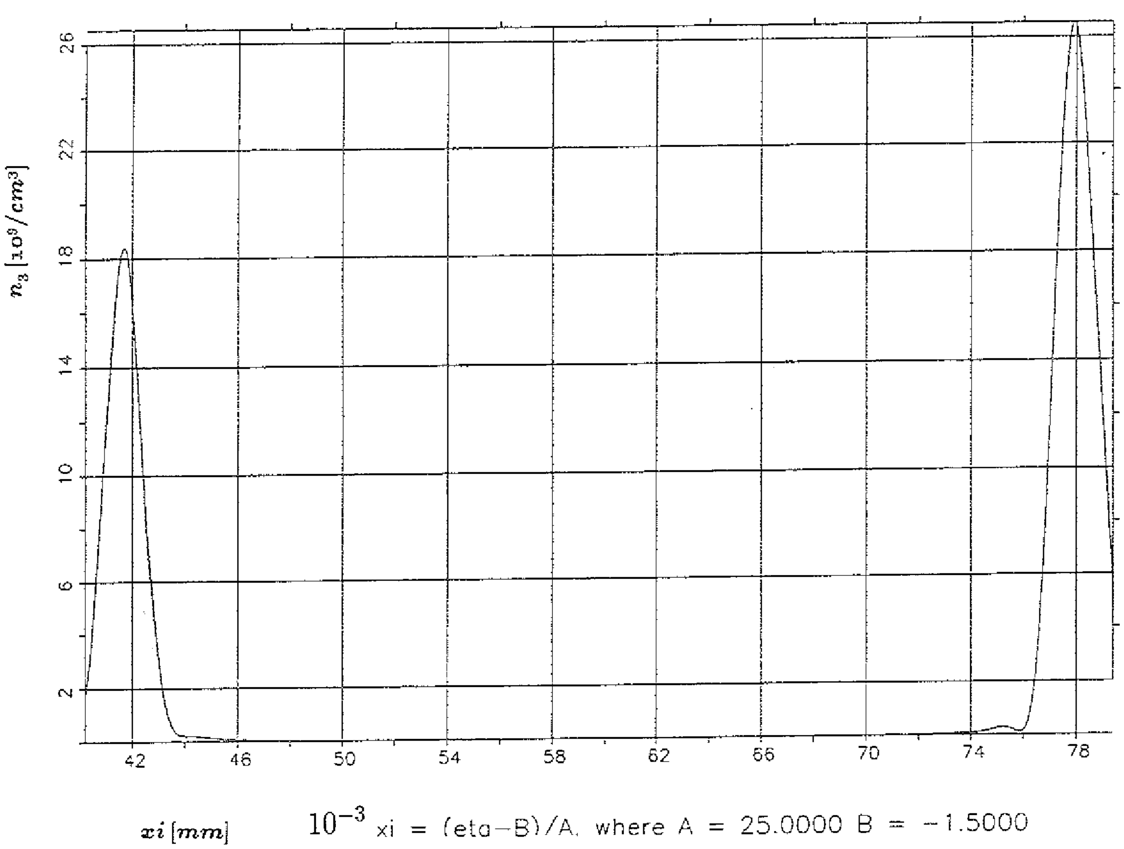

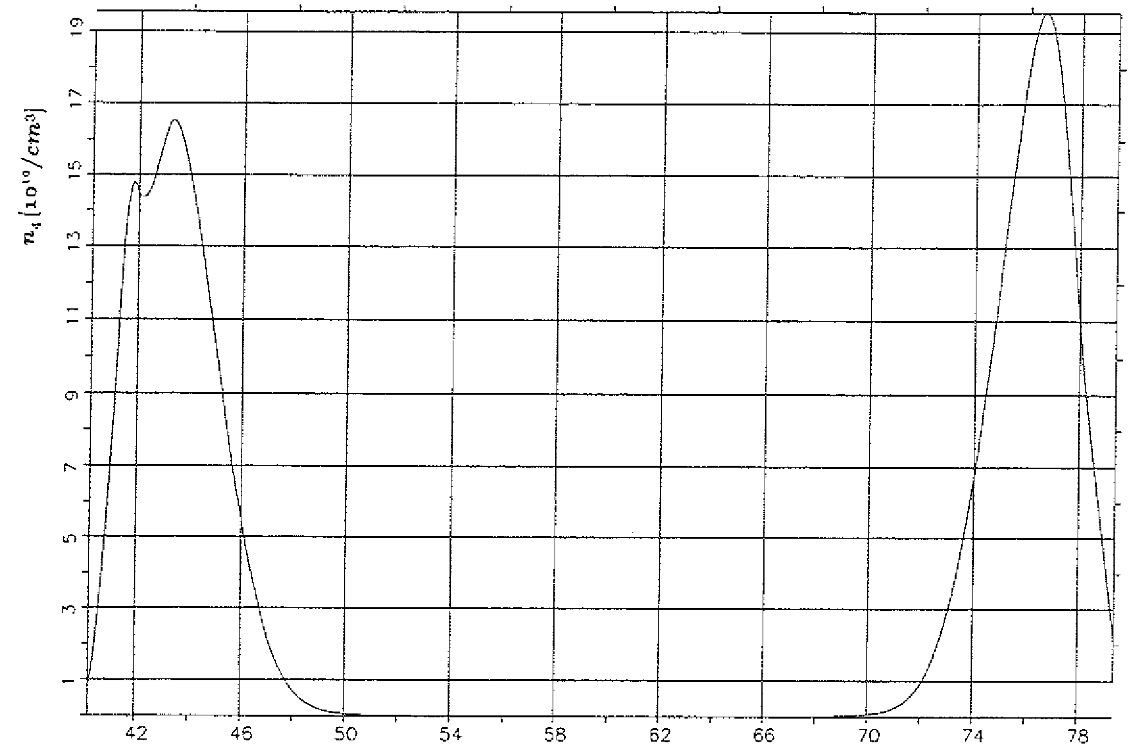

$xi\,[mm]$ 10^{-3} xi = (eta−B)/A, where A = 25.0000 B = −1.5000

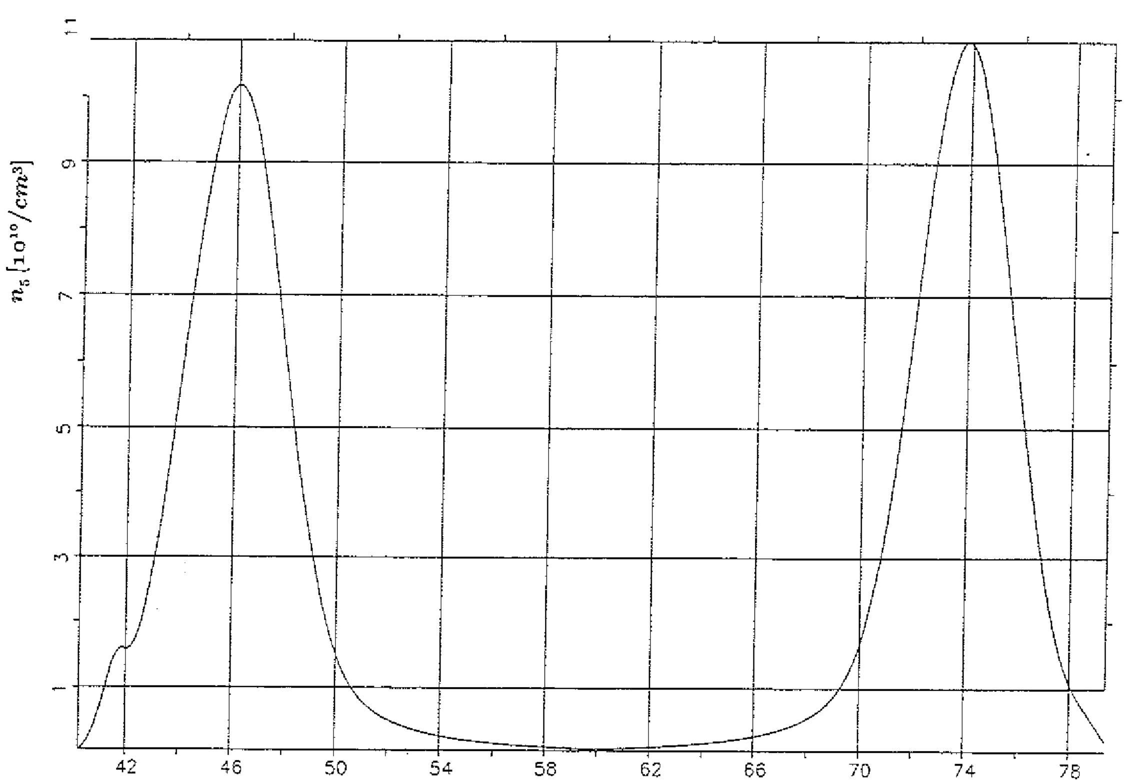

$xi\,[mm]$ 10^{-3} xi = (eta−B)/A, where A = 25.0000 B = −1.5000

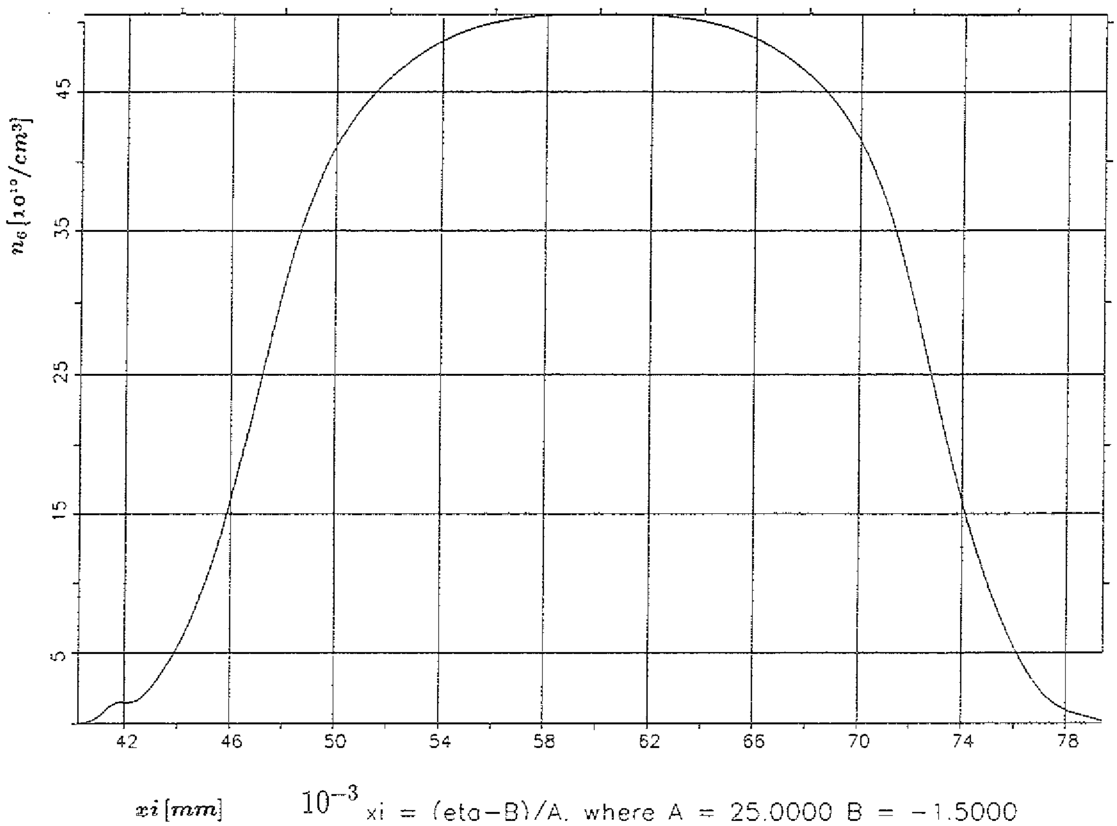
$n_6\,[10^{10}/cm^3]$
5
15
25
35
45
42
46
50
54
58
62
66
70
74
78
$xi\,[mm]$
10^{-3} xi = (eta−B)/A. where A = 25.0000 B = −1.5000

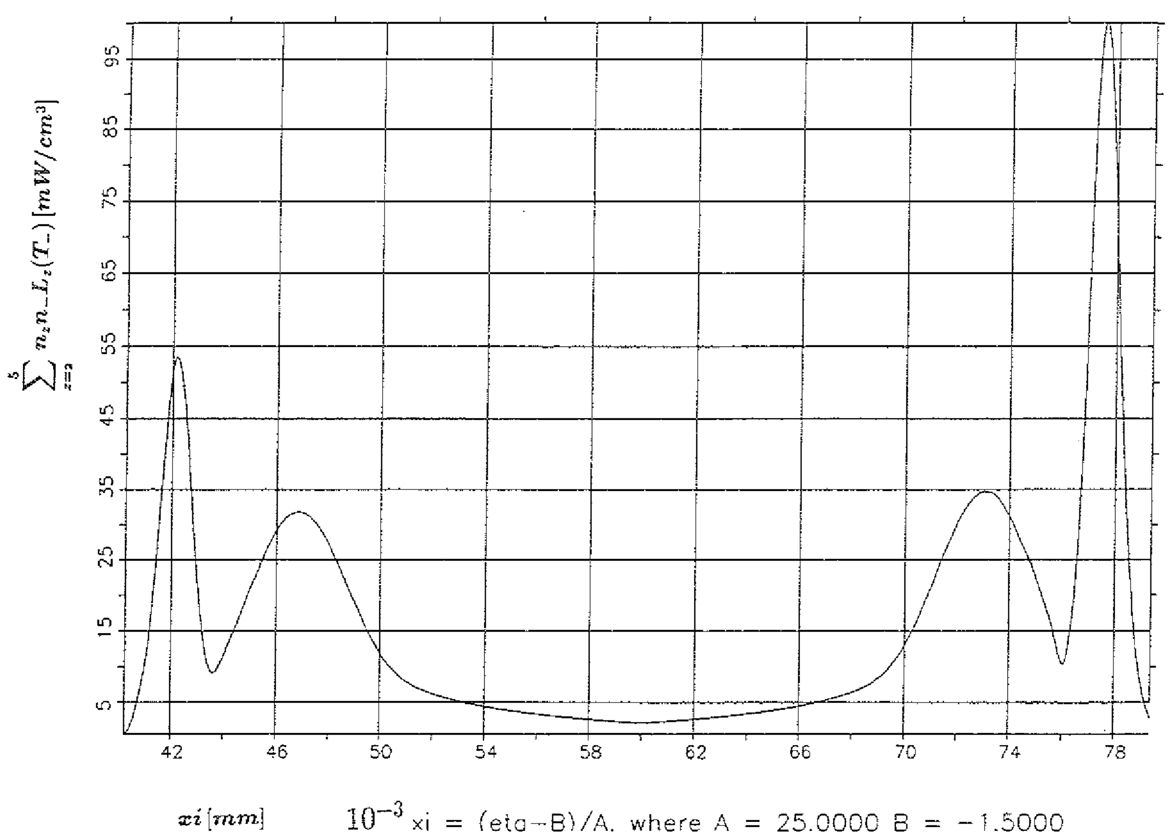
$\sum_{z=2}^{5} n_z n\_L_z(T\_)\,[mW/cm^3]$
5
15
25
35
45
55
65
75
85
95
42
46
50
54
58
62
66
70
74
78
$xi\,[mm]$
10^{-3} xi = (eta−B)/A. where A = 25.0000 B = −1.5000

Line integrated radiation densities of C^{z+} ($2 \leq z \leq 5$)

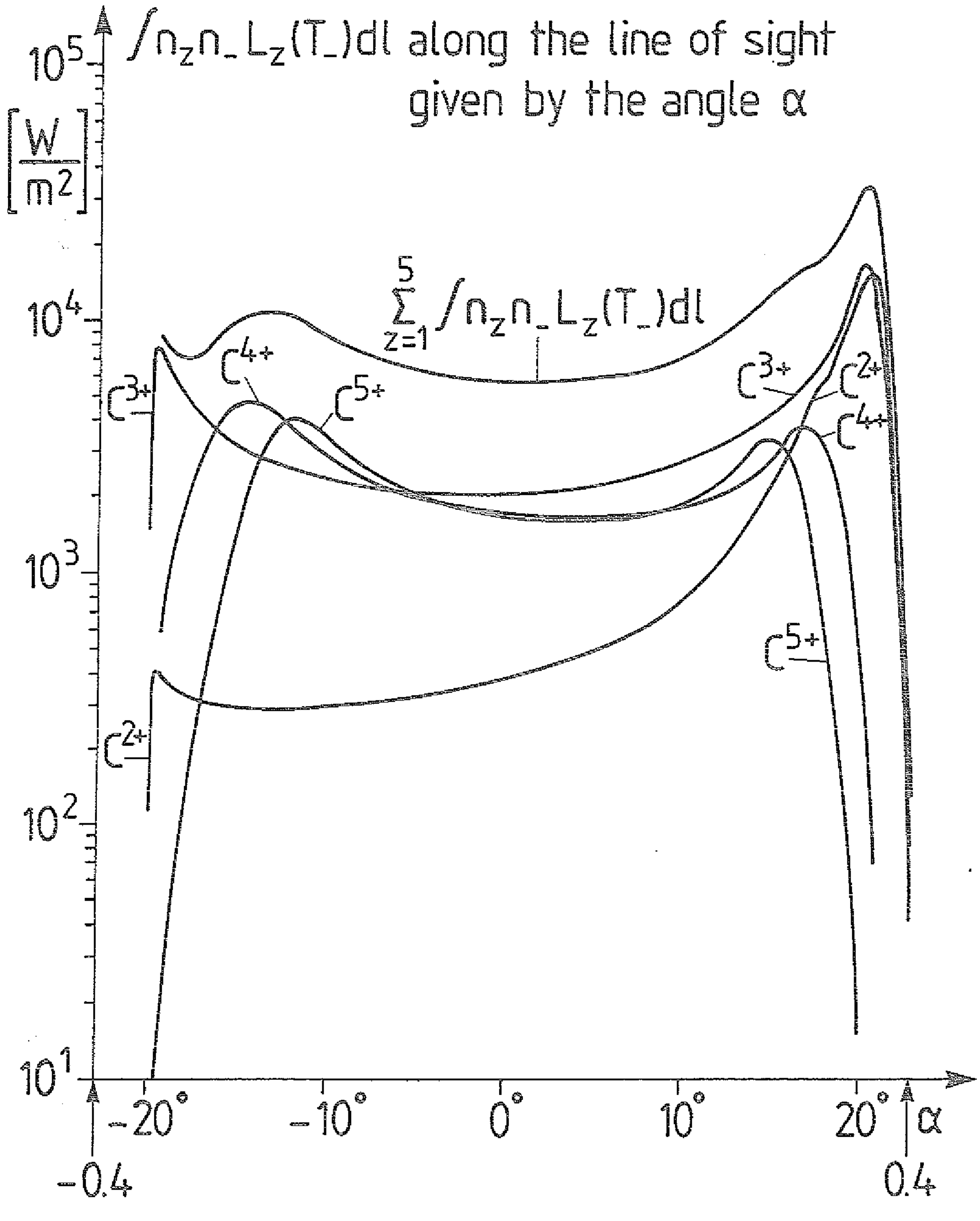

under sole consideration of the C^0 limiter source

KFA Jülich IPP	fig.7a	Gerhauser 1995 / 67-6187

Line integrated radiation densities of C^{z+} $(2 \leq z \leq 5)$

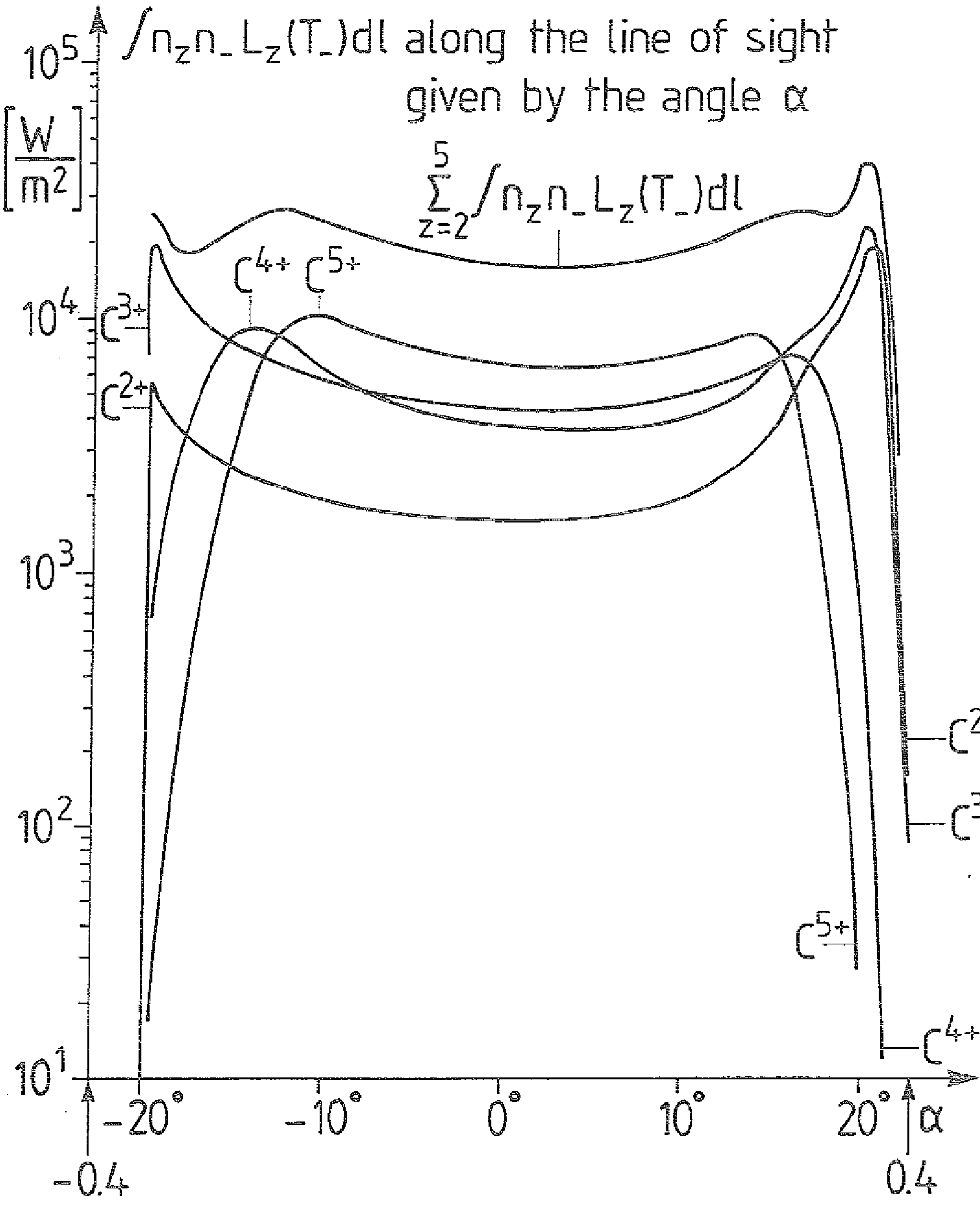

calculated for an additional uniform C^0 wall source

Jülich IPP	fig.7b	Gerhauser 1995 67 - 6188

Experimental set-up for UV-spectroscopy

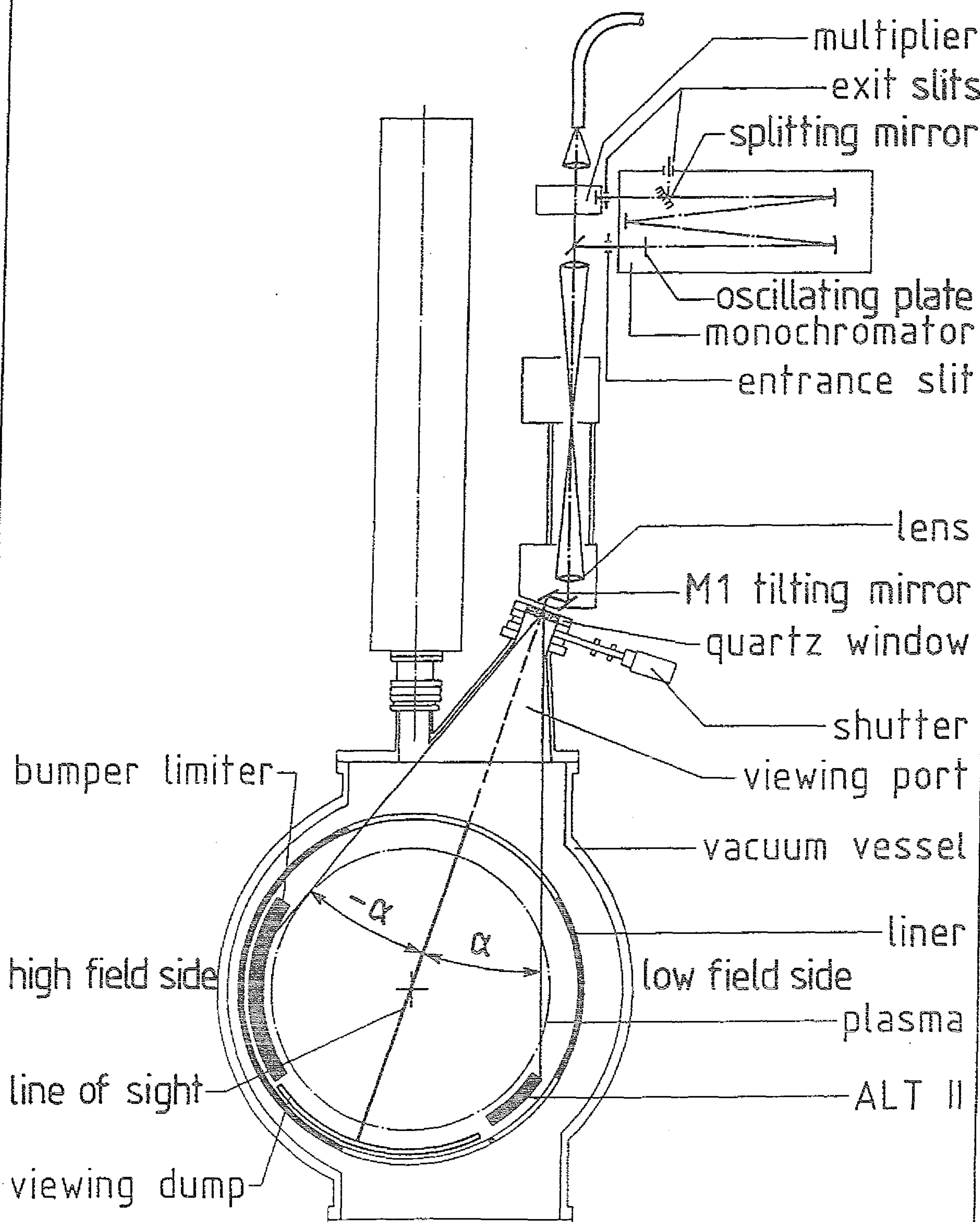

KFA Jülich IPP	fig.7c	Telesca 1992
		67 - 5610

Line radiation from C^{2+}, C^{3+} and C^{4+} ions emitted, respectively, at 229.6 nm (2s2p $^1P^0$–2p^2 ^1D), 253.0 nm (4f $^2F^0$–5g ^2G) and 227.1 nm (2s ^3S–2p $^3P^0$)

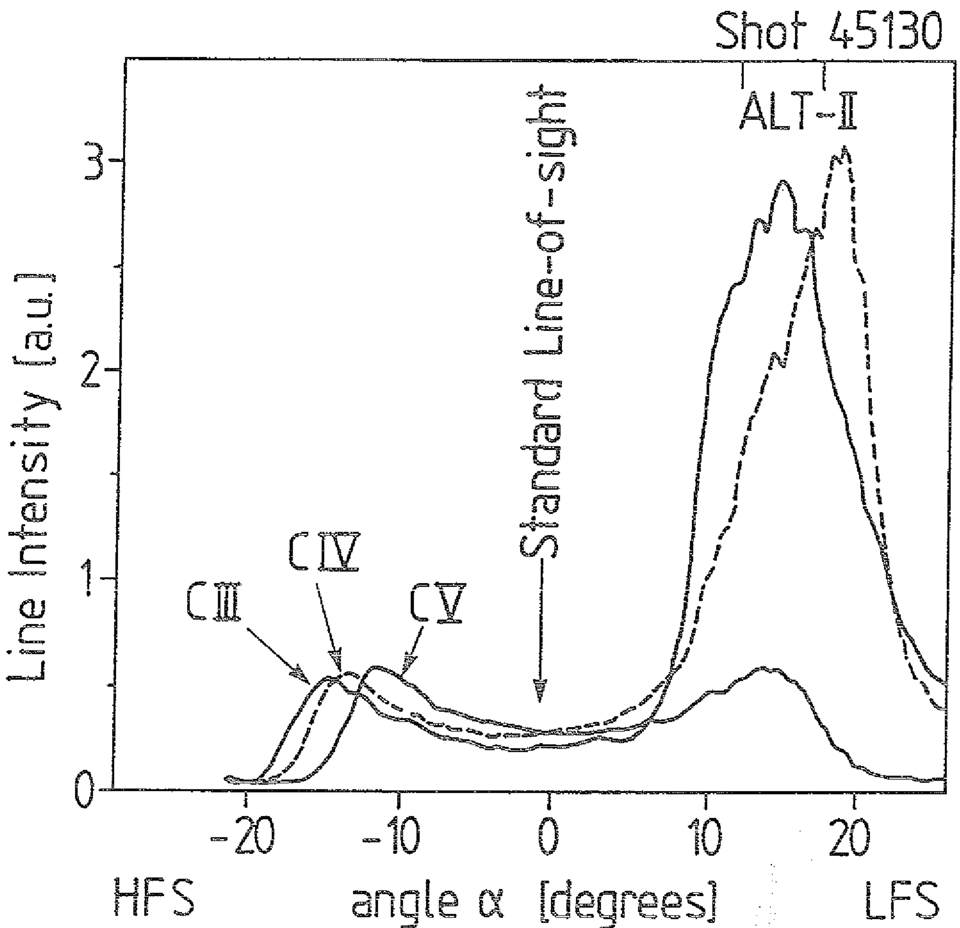

KFA Jülich IPP	**fig.7d**	Telesca 1993 / 67-5966

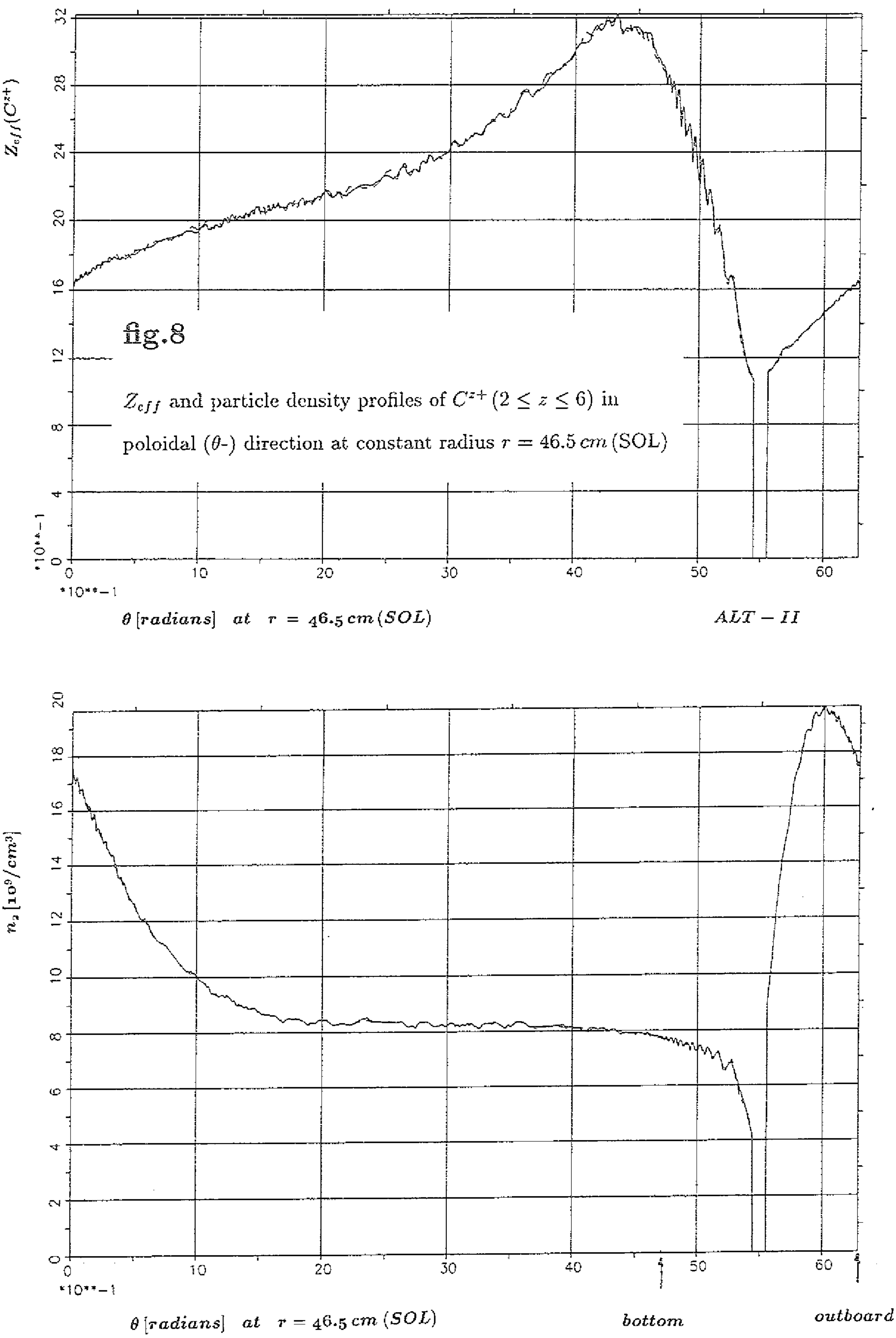

fig.8

Z_{eff} and particle density profiles of $C^{z+}\,(2 \leq z \leq 6)$ in poloidal (θ-) direction at constant radius $r = 46.5\,cm$ (SOL)

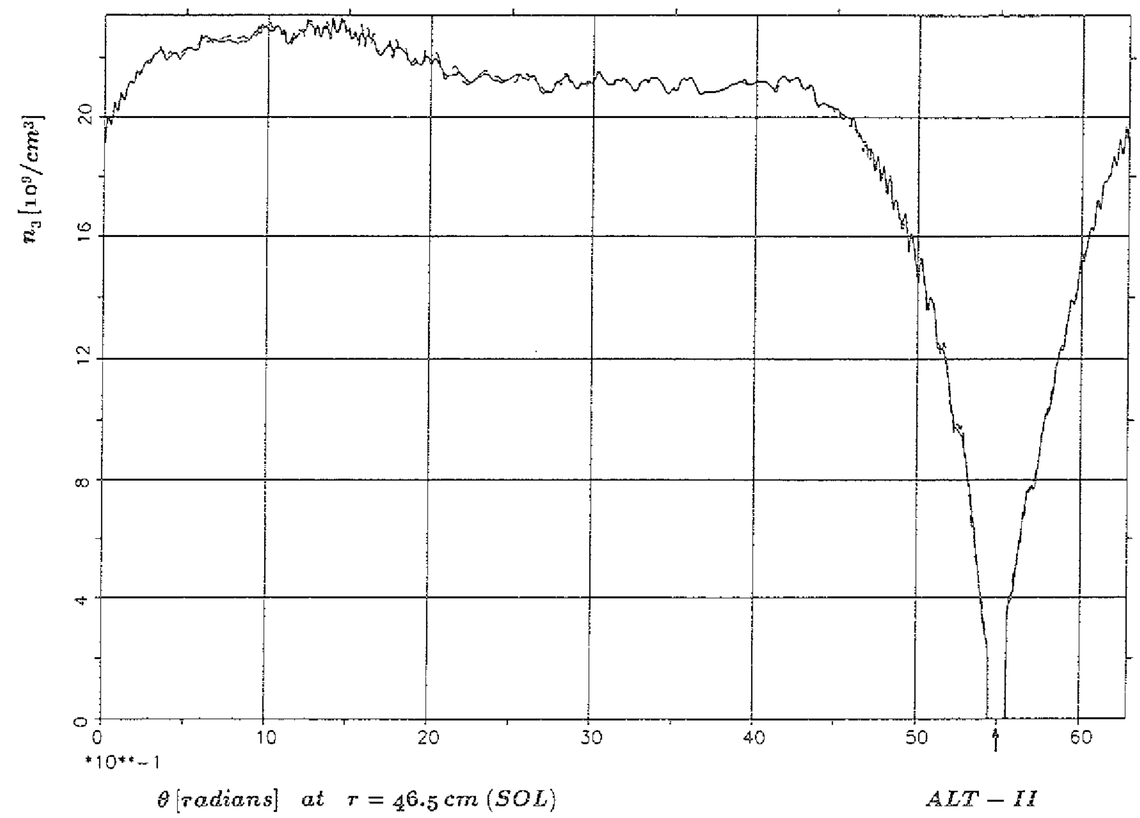

$n_3\,[10^9/cm^3]$
0
4
8
12
16
20
0
10
20
30
40
50
60
*10**-1
θ [radians] at $r = 46.5\,cm$ (SOL)
ALT − II

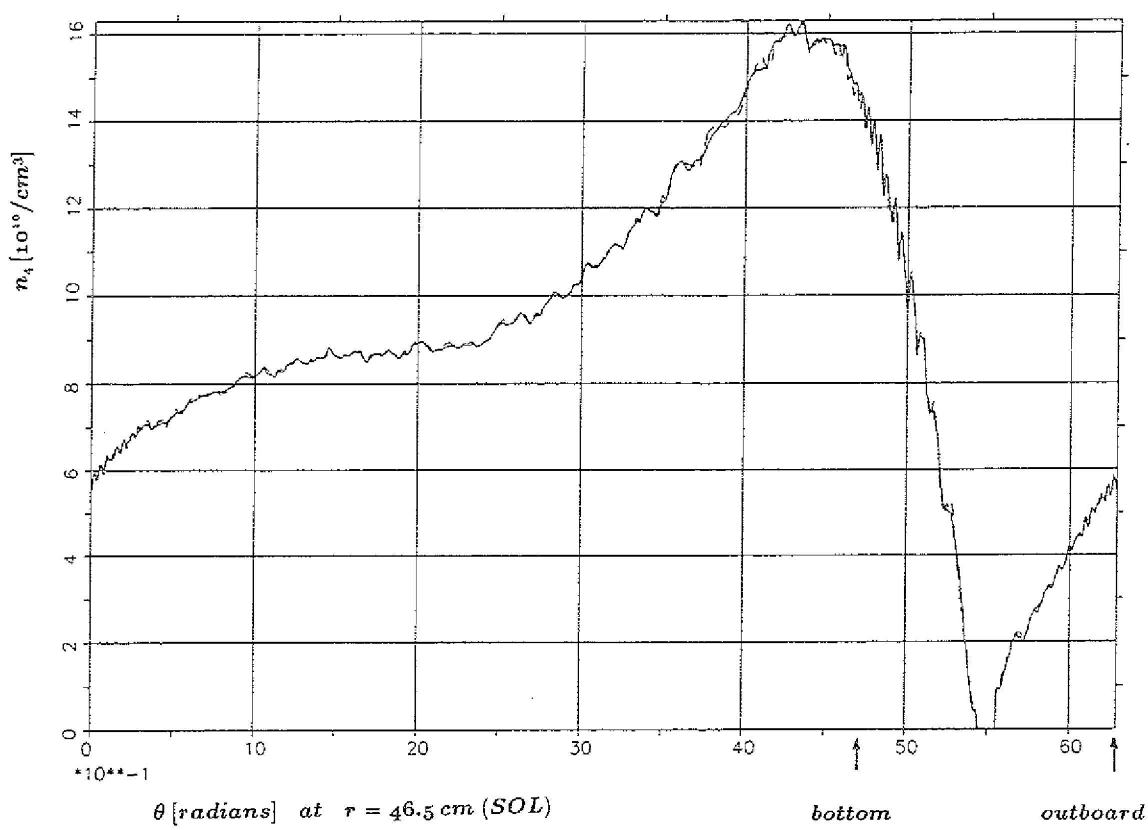

$n_4\,[10^{10}/cm^3]$
0
2
4
6
8
10
12
14
16
0
10
20
30
40
50
60
*10**-1
θ [radians] at $r = 46.5\,cm$ (SOL)
bottom
outboard

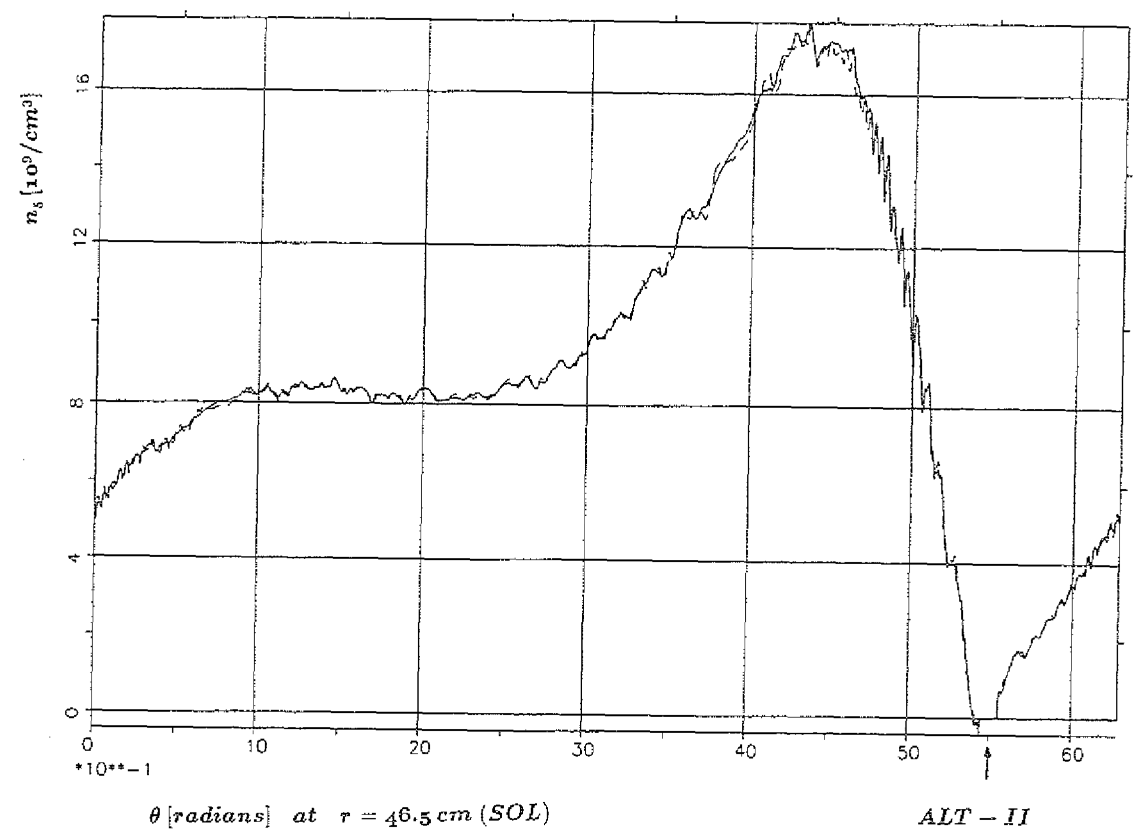
$n_s\,[10^9/cm^3]$
0
4
8
12
16
0
10
20
30
40
50
60
*10**-1
θ [radians] at $r = 46.5\,cm$ (SOL)
ALT – II

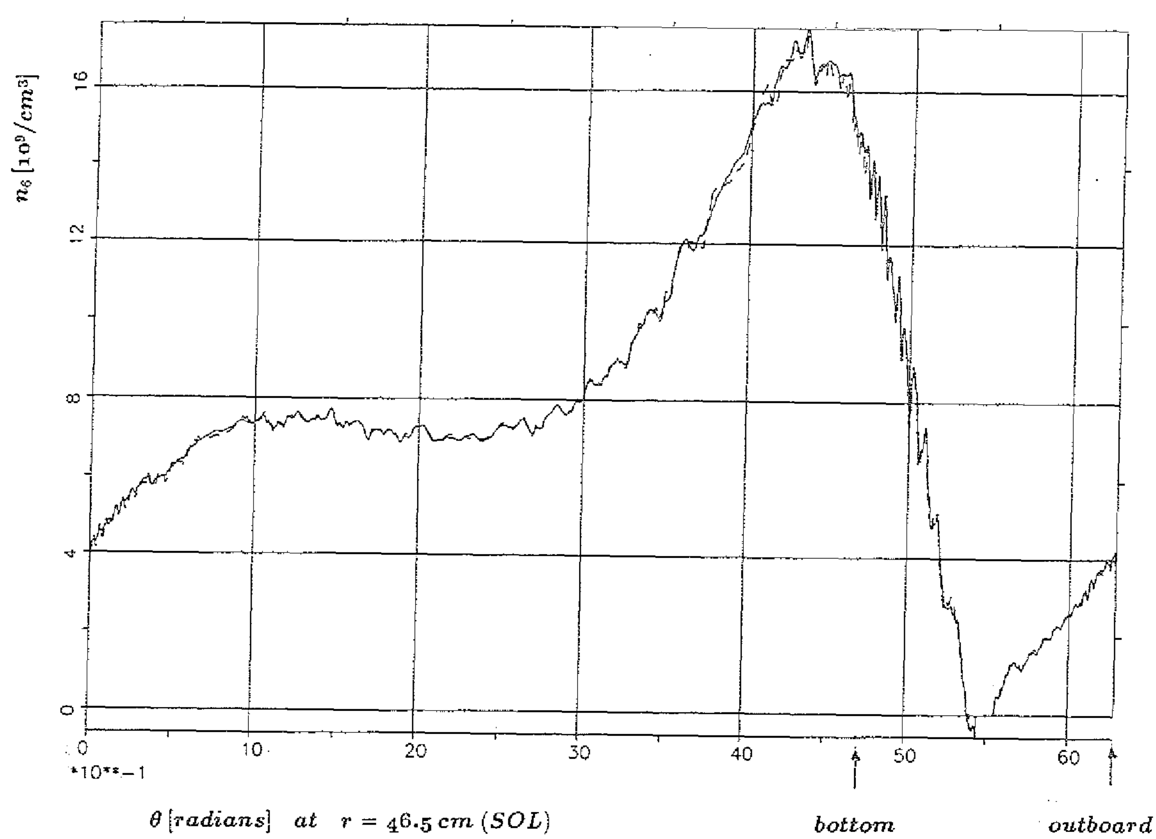
$n_6\,[10^9/cm^3]$
0
4
8
12
16
0
10
20
30
40
50
60
*10**-1
θ [radians] at $r = 46.5\,cm$ (SOL)
bottom
outboard

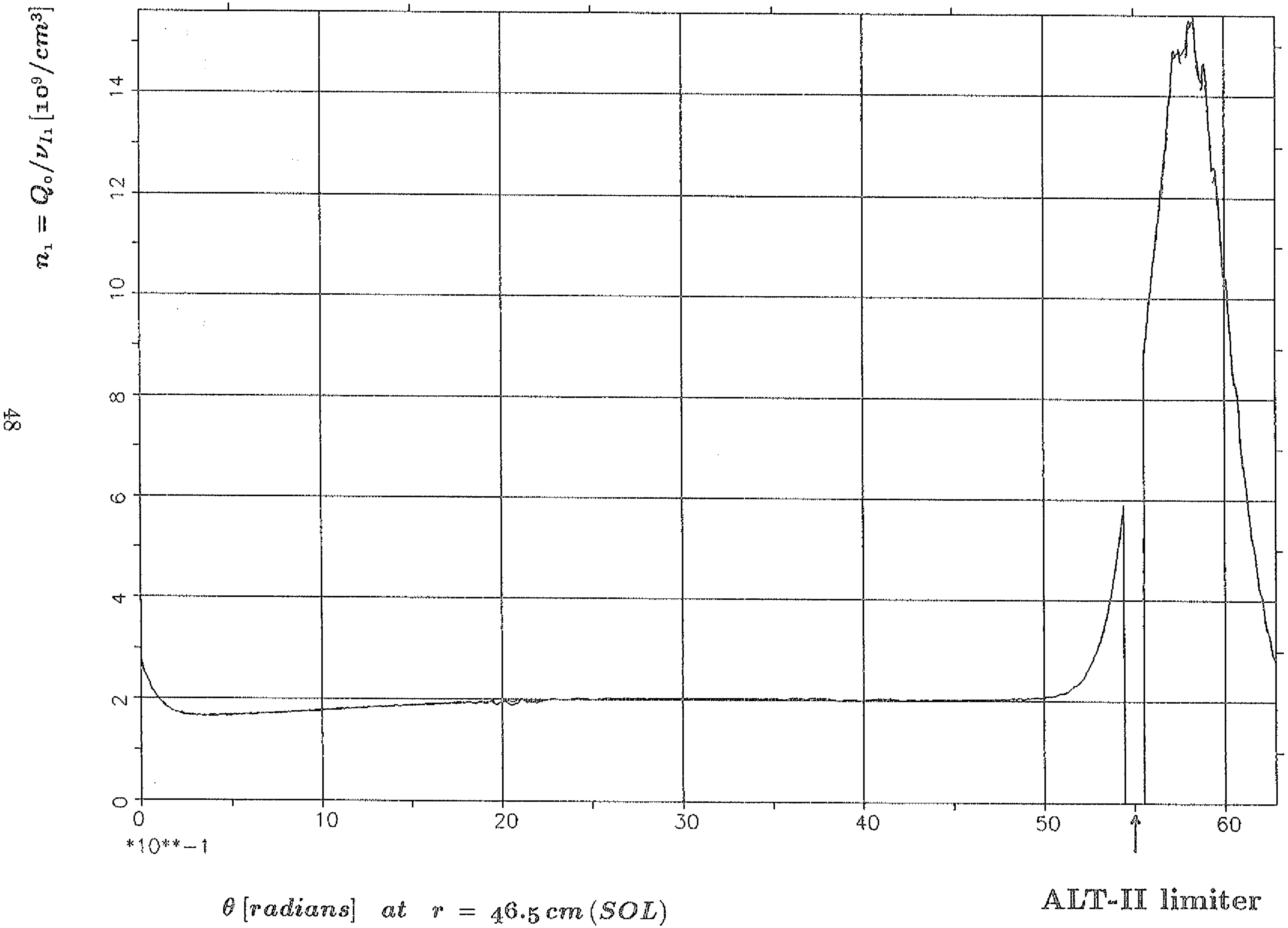

$n_1 = Q_0/\nu_{I1}$ [$10^9/cm^3$]
0
2
4
6
8
10
12
14
0
10
20
30
40
50
60
*10**-1
θ [radians] at r = 46.5 cm (SOL)
ALT-II limiter

FORSCHUNGSZENTRUM JÜLICH GmbH

Jül-3058
May 1995
ISSN 0944-2952